Conditional deletion of ferritin H in mice induces loss of iron storage and liver damage

Running Title: Conditional ferritin H deletion in mice

Deepak Darshan[1,3,4], Liviu Vanoaica[1,3], Larry Richman[1], Friedrich Beermann[2] and Lukas C. Kühn[1]

[1] Ecole Polytechnique Fédérale de Lausanne (EPFL), ISREC - Swiss Institute for Experimental Cancer Research, Lausanne, Switzerland

[2] Ecole Polytechnique Fédérale de Lausanne (EPFL), ISREC - Swiss Institute for Experimental Cancer Research, Transgenic mouse facility, Lausanne, Switzerland

[3] authors have equally contributed

[4] Present address: Queensland Institute of Medical Research, PO Royal Brisbane Hospital, Brisbane QLD 4029, Australia

Keywords: targeted gene deletion, Mx-Cre, hepcidin 1, macrophage, mouse embryonic fibroblast.

Corresponding author:

Dr. Lukas C. Kühn,

Ecole Polytechnique Fédérale de Lausanne (EPFL)

ISREC - Swiss Institute for Experimental Cancer Research,

SV2516 – Bâtiment SV, Station 19

CH-1015 Lausanne, Switzerland.

Tel: + 4121 - 692 58 36 (will change on March 18)

Fax: + 4121 – 652 69 33 (will change on March 18)

e-mail: lukas.kuehn@epfl.ch

List of Abbreviations:

IRP, iron regulatory protein; ROS, reactive oxygen species; ferritin H gene, *Fth* gene; TUNEL, transferase dUTP nick end labeling; ALT, alanine transaminase; AST, aspartate transaminase

Financial support: This work was supported by the Swiss Cancer League grant KFS 1000-02-2000 and the Swiss National Science Foundation grant 3100-065435.

Ferritin plays a central role in iron metabolism by acting both as iron storage and detoxifying protein. We have generated a ferritin H allele with loxP sites and studied the conditional ferritin H deletion in adult mice. Ten days after Mx-Cre induced deletion, ferritin H mRNA was below 5% in the liver, spleen and bone marrow of deleted mice compared to control littermates. Mice lost their cellular iron stores indicating the requirement of ferritin H in iron deposition. Serum iron and transferrin saturation were slightly increased and correlated with a 2-fold increased liver hepcidin 1 mRNA and a reduced duodenal DcytB mRNA level. Under normal iron regimen, deleted mice survived for 2 years without visible disadvantage. Mice fed on a high iron diet prior to ferritin H deletion suffered from severe liver damage. Similarly, ferritin H deleted mouse embryonic fibroblasts showed rapid cell death after exposure to iron salt in the medium. This was reversed by wildtype ferritin H but not by a ferritin H mutant lacking ferroxidase activity. Cell death was preceded by an increase in cytoplasmic free iron, reactive oxygen species, and mitochondrial depolarization. *Conclusion:* Our results provide evidence that the iron storage function of ferritin plays a major role in preventing iron-mediated cell and tissue damage.

Protein shells of 24 ferritin H and L subunits can accumulate up to 4500 iron atoms as Fe^{3+} in all tissues, but most prominently in hepatocytes and reticuloendothelial cells of liver and spleen.[1] The ferritin H subunit has a ferroxidase activity needed for iron deposition.[2,3] Translation of both subunits is regulated by iron regulatory proteins 1 and 2 (IRP1 and IRP2) in response to iron availability.[4] Thus, the amount of ferritin adapts to body iron levels. Iron stored in ferritin can be mobilized prior to ferritin degradation.[5] Ferritin's iron scavenging function is also thought to prevent iron-mediated catalysis of reactive oxygen species (ROS), which provoke tissue damage[6] and may cause cancer[7] and neurodegeneration.[8]

Previous studies in mice found that a straight knock-out of the ferritin H (*Fth*) gene provokes embryonic lethality.[9] Until now, this has hampered studying potential other functions of ferritin *in vivo*. Ferritin might contribute iron for cell proliferation of lymphoid cells[10] and complement extracellular iron uptake from transferrin by transferrin receptor.[11] Ferritin was also postulated to scavenge excess iron from nutrition in duodenal cells, known as the "mucosal block" hypothesis.[12,13] Under this hypothesis, when body iron stores are high and ferritin synthesis in crypt cells increased, mature villus cells might retain iron and prevent its basolateral release to serum. This view is not formally excluded, but challenged by the discovery of the peptide hormone hepcidin 1.[14,15] The relative importance of ferritin versus hepcidin 1 remains therefore to be investigated. Hepcidin 1 expression is regulated by body iron levels and essential for the control of iron absorption.[14-16] Hepcidin 1 may either repress mRNA of iron transporters through signaling[17,18] and/or interfere directly with basolateral iron export by binding to ferroportin.[19] Ferritin also retains iron in reticuloendothelial cells during anemia of acute or chronic inflammation, but it remains unknown whether ferritin synthesis is the cause or result of iron retention. Again, hepcidin 1, induced by inflammatory cytokines,

might favor iron retention by controlling iron efflux via ferroportin.[19,20] Finally, it was debated whether ferritin is important in providing iron for heme biosynthesis.[21,22]

Here we have generated mice carrying loxP sites 5' of the *Fth* gene promoter and 3' of exon 1 in order to delete ferritin H expression in adult mice by Cre recombinase. We have conditionally deleted the *Fth* gene in adult male mice using Cre under the control of the poly-IC inducible Mx gene promoter.[23] This deletes ferritin H almost completely in liver, bone marrow, spleen and thymus, but less prominently in other tissues. We report here the effects on iron storage, iron toxicity, hematological parameters and cell viability. We have explored effects of iron overload before or after ferritin H deletion and found rapid cell death in the liver and in mouse embryonic fibroblasts derived from our mice. In cultured cells, the cause of death could be attributed to ROS, mitochondrial depolarization and permeability transition.

Experimental procedures

All experimental procedures are accessible as “Supplementary Materials and Methods”.

Results

Conditional ferritin H deletion is lethal in embryos

To study the function of ferritin H in adult mice, we have generated, by embryonic stem cell recombination, mice with a modified ferritin H allele referred to as *Fth*^{loxNeo}. In this allele, the ferritin H promoter and exon 1 are bordered by loxP sites that also flank a neomycin selection cassette between FRT sites (Supplementary fig. 1). To verify our ferritin H targeting strategy, we crossed *Fth*^{loxNeo} mice with hemizygous nestin-Cre1 mice.[24] The nestin promoter shows a complex expression pattern with activity in the brain as well as in the germ line.[24] Therefore, complete deletion of ferritin H was expected to occur in *Fth*$^{loxNeo/+}$;*Nes-Cre1* animals. Of 38 F2 mice, 17 (44.7%) were *Fth*$^{+/+}$ and 21 (55.3%) were *Fth*$^{+/-}$ confirming nestin-Cre induced deletion. No *Fth*$^{-/-}$ mice were born indicating an essential function of ferritin H in embryogenesis. These results are best explained by a germ-line deletion of ferritin H in the *Fth*$^{loxNeo/+}$;*Nes-Cre1* F1 generation[24] with embryonic lethality when the *Fth* gene is absent from germ cells.[9] They are in agreement with previously published studies on embryonic lethality of ferritin deletion in mice.

Ferritin H deletion in adult animals induces loss of iron storage

For all subsequent experiments we used *Fth*$^{lox/lox}$ mice derived by breeding *Fth*$^{loxNeo/loxNeo}$ mice with mice transgenic for Flp recombinase. *Fth*$^{lox/lox}$ mice were crossed with transgenic Mx-Cre mice to obtain experimental *Fth*$^{lox/lox}$*;Mx-Cre* and control *Fth*$^{lox/lox}$ littermates. Initially, mice

were of mixed genetic background (C57 BL/6 x 129/Sv), but with advancement of the analysis, mice were 10 times backcrossed with C57BL/6J mice. Upon induction by poly I/C, the ferritin H gene deletion was analyzed in adult male mice (Fig. 1A). Liver, spleen and bone marrow showed an almost complete loss in the ferritin H gene and mRNA. In parallel, ferritin H protein was rapidly lost (Figs 1B and 1C). However, staining for ferritin L was enhanced (Fig. 1B), possibly due to increased ferritin L translation after IRP1 and IRP2 inactivation by iron liberated upon ferritin H degradation.[4] Concomitant with the loss of ferritin H mRNA, liver and spleen showed a marked decrease in tissue iron (Fig. 1A). In duodenum and heart, ferritin H mRNA was significantly reduced, but not enough to affect iron storage (Fig. 1A), whereas in kidney and lung, ferritin H was poorly deleted as expected.[23] Histochemical analysis showed also a complete loss of iron deposits in spleen reticuloendothelial cells of $Fth^{\Delta/\Delta}$ mice (Fig. 1D). This was not due to the loss of reticuloendothelial cells (Fig. 1E). Liver iron deposits were too low to be detected by this method, or by DAB-enhanced iron staining.

Ferritin is not required for hemoglobin synthesis

Most iron is recycled from hemoglobin of senescent erythrocytes, by the reticuloendothelial cells, and subsequently reincorporated into fresh hemoglobin in erythroid precursor cells. Therefore, it was of interest to observe whether Mx-Cre induced ferritin H deletion (Fig. 1A) would modify hemoglobin and hematocrit levels. $Fth^{\Delta/\Delta}$ mice showed no significant difference compared to $Fth^{lox/lox}$ mice (Supplementary table 1), and they survived for 2 years without noticeable disadvantage, while the extent of deleted cells remained unchanged. It suggests that ferritin H is not essential for iron recycling by macrophages and erythroid heme-biosynthesis. We further tested whether mice without ferritin H in liver and spleen showed changes in serum iron levels and transferrin saturation at 3, 10 and 30 days after ferritin H

deletion (Fig. 2B). A mild, but significant increase was observed for both parameters in experimental versus control mice.

Effects of Mx-Cre mediated ferritin H deletion on gene expression

Real-time PCR in *Fth*$^{\Delta/\Delta}$ versus *Fth*$^{lox/lox}$ mice at various time-points revealed a significant increase of liver hepcidin 1 mRNA (Fig. 2A). This increase correlated with increased serum iron (Fig. 2B) and transferrin saturation (Fig. 2C). Among mRNAs coding for proteins of duodenal iron transport, only Dcytb mRNA was significantly repressed, whereas mRNA of DMT1, ferroportin, and hephaestin showed no significant change (Fig. 2A and data not shown). Liver mRNAs of ferritin L, transferrin and Hfe were unchanged. Transferrin receptor 1 mRNA was slightly reduced in most tissues, compatible with mRNA destabilization due to IRP inactivation.[25] The mRNAs for transferrin receptor 2, superoxide dismutase 2 and glutathione peroxidase 1 remained unchanged in liver and intestine.

Severe liver damage by ferritin H deletion in animals with high iron diet

As *Fth*$^{\Delta/\Delta}$ mice on C57BL/6 background showed only mild changes, we investigated how well they would endure increased iron levels after feeding with iron-rich diet. As expected, they accumulated 8 times more iron in the liver and showed a 3.2-fold increase in hepcidin 1 mRNA (Figs 3B and C). Concomitantly, ferritin H was strongly induced (Fig. 3A, lane 2). Upon *Fth* gene deletion, ferritin H disappeared rapidly (Fig. 3A, lane 3) and tissue iron levels dropped to 39% within 5 days (Fig. 3B). Perl's staining of non-deleted liver sections showed diffuse iron staining in hepatocytes near blood vessels. Five days after deletion, the staining was weaker with a more granular appearance but no change in distribution (Fig 3G). Iron release from iron-loaded tissue did not sustain hepcidin 1 expression (Fig. 3C). Most prominently, these mice showed severe signs of illness and had to be sacrificed 5 days after

poly-IC injection. Their livers were swollen with a 42% increased wet weight. Liver tissue sections showed signs of irreversible cell damage with enlarged nuclei, macrosteatosis, hemorrhage and infiltration by polymorphonuclear cells (Fig 3E). Liver damage was confirmed by the terminal transferase dUTP nick end labeling (TUNEL) assay, which showed significantly more DNA strand breaks in iron-loaded $Fth^{\Delta/\Delta}$ mice than iron-loaded $Fth^{lox/lox}$ mice or mice on normal iron diet (Fig. 3F). Quantification of TUNEL staining in 7 fields of 4 independent animals (≅1500 cells) showed 9.4±5.3% stained cells for iron-loaded $Fth^{\Delta/\Delta}$ mice versus 1.8±0.4% for iron-loaded $Fth^{lox/lox}$ mice (p value<0.025). For normally fed $Fth^{\Delta/\Delta}$ and $Fth^{lox/lox}$ mice the values were 1.0±0.7% and 0.9±0.3%, respectively. Alanine transaminase (ALT) and aspartate transaminase (AST) activity in serum was also strongly increased (Fig. 3D). In addition, mRNA of heme oxygenase 1, a gene responding to oxidant signals, was induced 13-fold in iron-loaded $Fth^{\Delta/\Delta}$ versus $Fth^{lox/lox}$ mice. When non-loaded $Fth^{\Delta/\Delta}$ mice were injected with iron-dextran 2 months after ferritin H deletion, they showed the same acute liver damage as those pre-loaded with iron (not shown).

We questioned whether poly-IC was responsible for liver damage, possibly by triggering an inflammatory response. Therefore, we crossed $Fth^{lox/lox}$ mice with *SA-Cre-ER*^{T2} mice expressing tamoxifen-inducible Cre under control of the hepatocyte-specific serum albumin promoter, which leaves the ferritin H gene intact in liver macrophages.[26] Tamoxifen activation of Cre-ER^{T2} in 10-week old iron-loaded mice reduced liver ferritin H mRNA to 6-15% at day 10, reflecting the hepatocyte-specific deletion. Perl's staining prior to the deletion was similar to the one in $Fth^{lox/lox}$*;Mx-Cre* mice (Fig 3H). At day 10 after deletion, however, the staining in $Fth^{\Delta/\Delta}$*;SA-Cre-ER*^{T2} mice looked very different from the one in $Fth^{\Delta/\Delta}$*;Mx-Cre* mice. Noticably, hepatocytes did not show iron staining, but some iron remained highly concentrated in a few cells, which we identified as macrophages and in rare instances as

hepatocytes. Importantly, unlike *Fth*$^{\Delta/\Delta}$*;Mx-Cre* mice, the *Fth*$^{\Delta/\Delta}$*;SA-Cre-ER*^{T2} mice showed no signs of liver damage (Supplementary fig. 2). In order to create conditions similar to the Cre activation in Mx-Cre mice, poly-IC was injected together with tamoxifen. These mice showed again no signs of liver damage (not shown). We conclude that liver damage in *Fth*$^{\Delta/\Delta}$*;Mx-Cre* mice is not due to poly-IC, but rather iron toxicity.

Iron induced cell death of *Fth*$^{\Delta/\Delta}$ mouse embryonic fibroblasts

To study the mechanism of cellular iron toxicity, we derived *Fth*$^{\Delta/\Delta}$ and *Fth*$^{+/\Delta}$ mouse embryonic fibroblasts, which showed identical cell proliferation rates and viability in absence of iron salts. However, upon exposure to ferric ammonium citrate, *Fth*$^{\Delta/\Delta}$ cells were 30-fold more sensitive to iron (LD_{50}=1.3 μg/ml) than *Fth*$^{loxNeo/loxNeo}$ cells (LD_{50}=36 μg/ml) and 120-fold more than *Fth*$^{+/\Delta}$ cells (LD_{50}=151 μg/ml) (Fig. 4A). *Fth*$^{\Delta/\Delta}$ cell death could be rescued by wildtype ferritin H using an inducible vector (Fig. 4B). No rescue was observed upon expression of mutant ferritin H lacking ferroxidase activity (Fig. 4B). In all cell populations tested LD_{50} values correlated well with ferritin mRNA levels (Fig. 4C). Together, these data indicate an essential role of ferritin in the protection against iron toxicity.

To analyze directly whether increased cytoplasmic iron correlates with cell death, we measured IRP activity by an mRNA translation assay with unstable d2EGFP reporter linked to the 5'-iron responsive element of mouse ferritin L. In this assay, low cytoplasmic iron increases IRP activity, which represses d2EGFP translation. When free iron increases, IRP is inactivated and translation repression relieved. Thus, measuring d2EGFP steady state levels by FACS (Supplementary fig. 5) reflects cytoplasmic free iron levels. d2EGFP expression was increased 80% or more with iron concentrations at the LD_{50} or above. To reach an increased free iron pool, *Fth*$^{\Delta/\Delta}$ cells needed much lower extracellular iron concentrations than

Fth$^{loxNeo/loxNeo}$ cells (Fig. 5A). The increase in free iron correlated with an enhanced accumulation of ROS as measured by dichlorofluorescein (DCF) already 3h after the addition of ferric ammonium citrate to cells (Fig. 5B). After 16 h cells showed signs of mitochondrial depolarization and membrane permeability at or above the LD_{50} iron level (Fig. 5C and Supplementary fig. 6). Several inhibitors of oxidant activity were able to prevent mitochondrial depolarization and permeability transition (Fig. 5D). Notably mitoquinone diminished iron toxicity strongly. Cells also underwent mitochondrial permeability transition, which was clearly visible in *Fth*$^{loxNeo/loxNeo}$ cells exposed to high iron concentrations needed for mitochondrial depolarization (Supplementary fig. 7). This effect was, however, not visible in *Fth*$^{\Delta/\Delta}$ at lower iron concentrations, which nonetheless induced depolarization. It indicates that mitochondrial permeability transition was not a prerequisite for mitochondrial depolarization.

Discussion

Our data provide clear evidence for the requirement of ferritin H in iron storage and detoxification. We conclude that iron storage *in vivo* cannot be maintained by ferritin L alone. The importance of ferritin H and its ferroxidase activity for ferritin assembly and iron deposition was previously described *in vitro* and for cell lines with diminished or increased ferritin H levels.[27,28] Our results extend these studies to tissues under physiological conditions. As iron stores and ferritin H are rapidly reduced in deleted tissues, we conclude that ferritin is continuously degraded. This agrees with reports of ferritin half-lives of 3 days in rat liver[29] and <24 h in tissue culture cells.[30] Thus, iron stores are dynamic making the metal continuously available for the biosynthesis of iron-containing proteins. Upon *Fth* gene knock-out, iron cannot be redeposited into ferritin and leaves the tissue as observed for spleen and liver. It explains the increased serum iron and transferrin saturation. However, about 20 to 40% of the non-heme liver iron remained with a granular appearance, and further work is required to resolve the identity of these non-degradable iron deposits. Attempts to trace the redistribution of iron showed no significant increase in other tissues (Fig. 1A), possibly because C57BL/6 mice accumulate modest hepatic iron stores.[31] Studies using ^{59}Fe should detail this further.

Hepcidin 1 is central to the regulation of intestinal iron absorption and iron recycling from reticulocytes.[14-16,19,20] Our results showing a correlation between hepcidin 1 mRNA induction and the increase in serum iron and transferrin saturation seem to reflect an iron- or holo-transferrin-dependent signaling to the hepcidin 1 gene.[14,32] More surprising is the diminished hepcidin 1 mRNA expression in animals fed with high iron and then deleted of ferritin H (Fig. 3C). However, proper cell responsiveness and signaling to the hepcidin 1 gene might be

altered by severe liver damage. We and others have observed that isolated primary hepatocytes in cell culture show diminished hepcidin 1 mRNA expression and are unresponsive to ferric iron in the medium (L. Vanoaica, unpublished observation)[14,33] unless treated within few hours with iron-loaded holo-transferrin.[32]

The acute liver damage observed within just a few days of the ferritin H deletion in iron-loaded Mx-Cre mice can neither be attributed to iron loading alone, nor to activation of the interferon-α pathway by poly-IC, as control mice showed no signs of damage. Our results in the hepatocyte-specific SA-Cre-ER^{T2}-mediated ferritin H deletion with tamoxifen, or with tamoxifen plus poly-IC, also exclude that poly-IC alone provokes liver damage. Cell death appears, therefore, directly related to iron liberated upon ferritin H deletion and degradation. Whether liberated iron is sufficient to provoke liver damage or involves signals due to ferritin deletion in other tissues remains to be investigated. The fact that ferritin H deleted mice fed with normal diet for 2 months and then injected with iron dextran show acute liver failure, argues in favor of a direct effect of iron toxicity on liver cells. Interestingly, the hepatocyte-specific SA-Cre-ER^{T2}-mediated ferritin H deletion does not provoke damage (Supplementary fig. 2). This suggests that hepatocytes are protected because adjacent macrophages absorb large amounts of liberated iron (Fig. 3), which is not the case in Mx-Cre mice.

We have gained mechanistic insight into the cause of iron toxicity in embryonic fibroblasts and show again that ferritin H protects against iron toxicity (Fig. 4). The protection depends directly on the capacity of ferritin to store iron, since the ferritin H deletion can be rescued by wildtype ferritin H, but not a mutant which lost its ferroxidase activity and iron storage capacity.[3, 27] As a first consequence of the ferritin H deletion, the intracellular free iron pool is increased as assessed by the relief of translation regulation of an iron responsive element

containing GFP reporter construct (Fig.5). This completes previous conclusions drawn in K562 cells where ferritin H overexpression reduced the free iron pool.[34] Probably as a direct consequence, ROS increased rapidly within 3 h in *Fth*$^{\Delta/\Delta}$ cells, even at low extracellular iron concentrations. While the causative connection between free iron and ROS is well documented, we confirm that ferritin H expression is absolutely essential to prevent ROS formation. Others have shown that siRNA-mediated knock-down of ferritin H in K562 cells increased free iron and ROS production,[35] and rendered cells more sensitive to H_2O_2.[28] Moreover, ferritin H induction by NF-κB can counteract TNFα induced apoptosis by scavenging iron and preventing ROS formation.[6] We extend these previous observations to the death mechanism with evidence that mitochondrial depolarization and permeability transition precede cell death. Mitochondrial depolarization appears to be direct consequence of iron-mediated ROS formation as they show similar iron dose response curves with a marked difference between *Fth*$^{\Delta/\Delta}$ and *Fth*$^{loxNeo/loxNeo}$ cells. The causative relationship is further underlined by the time-delay between ROS formation and mitochondrial depolarization, as well as the fact that inhibitors with anti-oxidant functions inhibit mitochondrial depolarization significantly. Iron was previously implicated in cold-induced apoptosis and shown to trigger mitochondrial permeability transition in hepatocytes.[36] ROS and mitochondrial permeability transition plays also a role in ischemia-reperfusion injury and iron poisoning.[37] Whether the liver damage observed in our Mx-Cre deleted mice is a direct consequence of mitochondrial depolarization remains to be studied. Our mice should become particularly useful to evaluate the role of iron-catalyzed ROS in specific tissues, and to establish the function of ferritin not only in acute iron toxicity, but also in long-term protection against DNA mutagenesis and aging.

References

1. Harrison PM, Arosio P. The ferritins: molecular properties, iron storage function and cellular regulation. Biochim. Biophys. Acta 1996;1275:161-203.
2. Levi S, Luzzago A, Cesareni G, Cozzi A, Franceschinelli F, Albertini A, Arosio P. Mechanism of ferritin uptake: activity of the H-chain and deletion mapping of the ferro-oxidase site. A study of iron uptake and ferro-oxidase activity of human liver, recombinant H-chain ferritins, and of two H-chain deletion mutants. J. Biol. Chem. 1988;263:18086-18092.
3. Lawson DM, Treffry A, Artymiuk PJ, Harrison PM, Yewdall SJ, Luzzago A, Cesareni G, et al. Identification of the ferroxidase centre in ferritin. FEBS Lett. 1989;254:207-210.
4. Hentze MW, Kühn LC. Molecular control of vertebrate iron metabolism - mRNA-based regulatory circuits operated by iron, nitric oxide, and oxidative stress. Proc. Natl Acad. Sci. USA 1996;93:8175-8182.
5. De Domenico I, Vaughn MB, Li LT, Bagley D, Musci G, Ward DW, Kaplan J. Ferroportin-mediated mobilization of ferritin iron precedes ferritin degradation by the proteasome. EMBO J. 2006;22:5396-5404.
6. Pham CG, Bubici C, Zazzeroni F, Papa S, Jones J, Alvarez K, Jayawardena S, et al. Ferritin heavy chain upregulation by NF-κB inhibits TNFα-induced apoptosis by suppressing reactive oxygen species. Cell 2004;119:529-542.
7. Hussain SP, Hoseth LJ, Harris CC. Radical causes of cancer. Nat. Rev. Cancer 2003;3:276-285.
8. Zecca L, Youdim MB, Riederer P, Connor JR, Crichton RR. Iron, brain ageing and neurodegenerative disorders. Nat. Rev. Neurosci. 2004;5:863-873.
9. Ferreira C, Bucchini D, Martin ME, Levi S, Arosio P, Grandchamp B, Beaumont C. Early embryonic lethality of H ferritin gene deletion in mice. J. Biol. Chem. 2000;275:3021-3024.
10. Golding S, Young SP. Iron Requirements of Human-Lymphocytes - Relative Contributions of Intracellular and Extracellular Iron. Scand. J. Immunol. 1995;41:229-236.
11. Ned RM, Swat W, Andrews NC. Transferrin receptor 1 is differentially required in lymphocyte development. Blood 2003;102:3711-3718.
12. Hahn PF, Bale WF, Ross JF, Balfour WM, Whipple GH. Radioactive iron absorption by gastro-intestinal tract. Influence of anemia, anoxia and antecedent feeding. Distribution in growing dogs. J. Exp. Med. 1943;78:169-188.

13. Granick S. Ferritin IX. Increase of the protein apoferritin in the gastrointestinal mucosa as a direct response to iron feeding. The function of ferritin in the regulation of iron absorption. J. Biol. Chem. 1946;164:737-746.
14. Pigeon C, Ilyin G, Courselaud B, Leroyer P, Turlin B, Brissot P, Loreal O. A new mouse liver-specific gene, encoding a protein homologous to human antimicrobial peptide hepcidin, is overexpressed during iron overload. J. Biol. Chem. 2001;276:7811-7819.
15. Nicolas G, Bennoun M, Devaux I, Beaumont C, Grandchamp B, Kahn A, Vaulont S. Lack of hepcidin gene expression and severe tissue iron overload in upstream stimulatory factor 2 (*USF2*) knockout mice. Proc. Natl Acad. Sci. USA 2001;98:8780-8785.
16. Roetto A, Papanikolaou G, Politou M, Alberti F, Girelli D, Christakis J, Loukopoulos D, et al. Mutant antimicrobial peptide hepcidin is associated with severe juvenile hemochromatosis. Nature Genet. 2003;33:21-22.
17. Zoller H, Koch RO, Theurl I, Obrist P, Pietrangelo A, Montosi G, Haile DJ, et al. Expression of the duodenal iron transporters divalent-metal transporter 1 and ferroportin 1 in iron deficiency and iron overload. Gastroenterology 2001;120:1412-1419.
18. Frazer DM, Wilkins SJ, Becker EM, Vulpe CD, McKie AT, Trinder D, Anderson GJ. Hepcidin expression inversely correlates with the expression of duodenal iron transporters and iron absorption in rats. Gastroenterology 2002;123:835-844.
19. Nemeth E, Tuttle MS, Powelson J, Vaughn MB, Donovan A, Ward DM, Ganz T, et al. Hepcidin regulates cellular iron efflux by binding to ferroportin and inducing its internalization. Science 2004;306:2090-2093.
20. Weinstein DA, Roy CN, Fleming MD, Loda MF, Wolfsdorf JI, Andrews NC. Inappropriate expression of hepcidin is associated with iron refractory anemia: implications for the anemia of chronic disease. Blood 2002;100:3776-3781.
21. Vaisman B, Fibach E, Konijn AM. Utilization of intracellular ferritin iron for hemoglobin synthesis in developing human erythroid precursors. Blood 1997;90:831-838.
22. Ponka P, Richardson DR, Konijn AM, Gelvan D, E. M-H, Fibach E. Can ferritin provide iron for hemoglobin synthesis? Blood 1997;89::2611-2613.
23. Kühn R, Schwenk F, Aguet M, Rajewsky K. Inducible gene targeting in mice. Science 1995;269:1427-1429.

24. Dubois NC, Hofmann D, Kaloulis K, Bishop JM, Trumpp A. Nestin-Cre transgenic mouse line Nes-Cre1 mediates highly efficient Cre/IoxP mediated recombination in the nervous system, kidney, and somite-derived tissues. Genesis 2006;44:355-360.

25. Müllner EW, Neupert B, Kühn LC. A specific mRNA-binding factor regulates the iron-dependent stability of cytoplasmic transferrin receptor mRNA. Cell 1989;58:373-382.

26. Schuler M, Dierich A, Chambon P, Metzger D. Efficient temporally controlled targeted somatic mutagenesis in hepatocytes of the mouse. Genesis 2004;39:167-172.

27. Santambrogio P, Levi S, Cozzi A, Corsi B, Arosio P. Evidence that the specificity of iron incorporation into homopolymers of human ferritin L- and H-chains is conferred by the nucleation and ferroxidase centres. Biochem. J. 1996;314:139-144.

28. Cozzi A, Corsi B, Levi S, Santambrogio P, Biasiotto G, Arosio P. Analysis of the biologic functions of H- and L-ferritins in HeLa cells by transfection with siRNAs and cDNAs: evidence for a proliferative role of L-ferritin. Blood 2004;103:2377-2383.

29. Drysdale JW, Munro HN. Regulation of synthesis and turnover of ferritin in rat liver. J. Biol. Chem. 1966;241:3630-3637.

30. Kidane TZ, Sauble E, Linder MC. Release of iron from ferritin requires lysosomal activity. Am. J. Physiol. Cell Physiol. 2006;291:C445-C455.

31. Fleming RE, Holden CC, Tomatsu S, Waheed A, Brunt EM, Britton RS, Bacon BR, et al. Mouse strain differences determine severity of iron accumulation in Hfe knockout model of hereditary hemochromatosis. Proc. Natl Acad. Sci. USA 2001;98:2707-2711.

32. Lin L, Valore EV, Nemeth E, Goodnough JB, Gabatan V, Ganz T. Iron transferrin regulates hepcidin synthesis in primary hepatocyte culture through hemojuvelin and BMP2/4. Blood 2007;110:2182-2189.

33. Nemeth E, Valore EV, Territo M, Schiller G, Lichtenstein A, Ganz T. Hepcidin, a putative mediator of anemia of inflammation, is a type II acute-phase protein. Blood 2003;101:2461-2463.

34. Picard V, Epsztejn S, Santambrogio P, Cabantchik ZI, Beaumont C. Role of ferritin in the control of the labile iron pool in murine erythroleukemia cells. J. Biol. Chem. 1998;273:15382-15386.

35. Kakhlon O, Gruenbaum Y, Cabantchik ZL. Repression of ferritin expression increases the labile iron pool, oxidative stress, and short-term growth of human erythroleukemia cells. Blood 2001;97:2863-2871.

36. Rauen U, Petrat F, Sustmann R, de Groot H. Iron-induced mitochondrial permeability transition in cultured hepatocytes. J. Hepatol. 2004;40:607-615.

37. Kroemer G, Galluzzi L, Brenner C. Mitochondrial membrane permeabilization in cell death. Physiol. Rev. 2007;787:99-163.

Acknowledgements

We thank Olav Zilian, Fabienne Seiler and Michel Aguet for advice and the Mx-Cre mouse, Andreas Trumpp for the Nes-Cre1 mouse and pKI-Cre ER^T, and Daniel Metzger and Pierre Chambon for the SA-Cre-ER^{T2} mouse, Michael Murphy for mitoquinone and Michael Reth for pAN-MerCreMer. We thank Sanjiv Luther for the macrophage staining in spleen and the MIM facility of ISREC for histology.

Figure legends

Figure 1. Conditional ferritin H deletion by Mx-Cre reduces iron storage in liver and spleen. Ten week old *Fth*$^{lox/lox}$*;Mx-Cre* and control *Fth*$^{lox/lox}$ mice were injected with poly-IC to activate Cre expression. **A.** At day 10, the ferritin H deletion was assessed in different tissues by real-time PCR on genomic DNA (green) and ferritin H cDNA (blue). Tissue iron content (red) was measured by the bathophenanthroline method. Values in *Fth*$^{\Delta/\Delta}$ mice (n=4) are expressed in % of values in *Fth*$^{lox/lox}$ mice (n=4) set as 100% ± standard deviation (SD). **B.** Immunofluorescence staining of ferritin H and L in frozen liver sections (day 10). Scale bar, 200 μm. **C.** Immunoblot analysis of liver ferritin H in one *Fth*$^{lox/lox}$ mouse and two *Fth*$^{\Delta/\Delta}$ mice at days 3 and 10. **D.** Frozen spleen sections stained by Perl's Prussian blue at day 30. Scale bar, 200 μm. **E.** Frozen spleen sections stained for macrophages with anti-CD11b and anti-F4/80 antibodies, as well as 4',6-diamidino-2-phenylindole (DAPI). Scale bar, 100 μm.

Figure 2. Ferritin H deletion causes increase of serum iron, transferrin saturation and liver hepcidin 1 mRNA, and repression of duodenal Dcytb mRNA. A. mRNA expression was tested by real-time PCR at days 3, 10 and 30 after ferritin H deletion using primers indicated in Supplementary table 2. Average expression (arbitrary units) for *Fth*$^{lox/lox}$ mice (n=6;3;3) and *Fth*$^{\Delta/\Delta}$ mice (n=6;3;3) was normalized to the geometric average of 2 control genes (GAPDH and HPRT in liver; GAPDH and β-actin in intestine) ± SD. *** $p<0.0005$; * $p<0.05$. **B.** Serum iron levels and transferrin saturation. * $p<0.05$. **C.** Transferrin saturation correlated with hepcidin 1 mRNA expression in *Fth*$^{lox/lox}$ (○) and *Fth*$^{\Delta/\Delta}$ (●) mice ($R=0.701$ and $p<0.0002$).

Figure 3. Severe physiological consequences of ferritin H deletion in iron-loaded mice. Mice were fed 14 days with 2.5% carbonyl iron diet prior to Mx-Cre induction and analyzed at day 5. **A.** Immunoblot of liver proteins probed with anti-ferritin H and control anti γ-tubulin antibodies. **B.** Liver iron in $Fth^{lox/lox}$ mice without (−Fe) (n=4) or with (+Fe) high iron diet (n=4) was compared to iron-loaded $Fth^{\Delta/\Delta}$ mice (n=4). **C.** Hepcidin 1 mRNA (arbitrary units) of the same mice as in B. was normalized to TATA box binding protein mRNA. **D.** Cytoplasmic liver enzyme activity of alanine transaminase (ALT) and aspartate transaminase (AST) in serum. *** $p<0.0005$; ** $p<0.005$; * $p<0.05$. **E.** Morphological changes in liver tissue sections stained with hematoxylin-eosin of iron-loaded $Fth^{lox/lox}$ (a) and $Fth^{\Delta/\Delta}$ mice (b to d) analyzed at day 5. Scale bar 100 μm. The sections of $Fth^{\Delta/\Delta}$ mice show extensive macrosteatosis (b), hemorrhage (c) and polymorphonuclear cell infiltration (d) with neutrophils (insert; scale bar 5 μm). Enlarged version in Supplementary fig. 3. **F.** TUNEL assay on frozen liver sections from normal and iron-loaded $Fth^{lox/lox}$ and $Fth^{\Delta/\Delta}$ mice. Iron-loaded $Fth^{\Delta/\Delta}$ mice (d) show significantly more apoptotic or necrotic nuclei with DNA strand breaks. Scale bar 100 μm. **G.** Perl's Prussian blue staining of liver in iron-loaded $Fth^{lox/lox}$ and $Fth^{\Delta/\Delta}$ mice at day 5 after Mx-Cre activation by poly-IC. Scale bar 200 μm. **H.** Perl's Prussian blue staining of liver in iron-loaded $Fth^{lox/lox}$ and $Fth^{\Delta/\Delta}$ mice at day 10 after SA-Cre-ER^{T2} activation with tamoxifen. Scale bar 200 μm. Enlarged version of panel **G** and **H** in Supplementary fig. 4.

Figure 4. Survival of mouse embryonic fibroblasts in iron-rich medium depends on the presence of functional ferritin H. Mouse embryonic fibroblasts were derived from $Fth^{loxNeo/loxNeo}$ and $Fth^{+/loxNeo}$ mice, transfected with CMV-Cre-ER^{T} and exposed to tamoxifen to derive $Fth^{\Delta/\Delta}$ and $Fth^{+/\Delta}$ cells. **A.** $Fth^{\Delta/\Delta}$ (○), $Fth^{loxNeo/loxNeo}$ (●) and $Fth^{+/\Delta}$ (◊) cells were incubated with increasing concentrations of ferric ammonium citrate and cell viability

measured after 4 days by the MTS assay. **B.** *Fth*$^{\Delta/\Delta}$ cells were transfected with cDNA of wildtype ferritin H (■) or a ferritin H without ferroxidase activity due to 62E→K and 65H→G mutations (□). Iron toxicity was assessed as in A. **C.** Correlation between ferritin H mRNA expression and LD_{50} dose of ferric ammonium citrate.

Figure 5. Iron toxicity in mouse embryonic fibroblasts involves increased cytoplasmic iron levels, ROS formation, and mitochondrial depolarization. A. *Fth*$^{loxNeo/loxNeo}$ (●) and *Fth*$^{\Delta/\Delta}$ (○) cells were infected with pSH-FTL-d2EGFP and unstable d2EGFP expression analyzed by the FACS at different iron concentrations (Supplementary fig. 5). Values report the fluorescence increase in d2EGFP-positive cells compared to conditions without iron addition (n=5). **B.** ROS formation was assessed by dichlorofluorescein (DCF) at 3, 6 and 16 h with different iron concentrations (n=3). **C.** Cells were stained at 6 or 16 h after ferric ammonium citrate addition with tetramethyl rhodamine methyl ester (TMRM) for mitochondrial depolarization (black bars) and 7-amino-actinomycin D (7aaD) for loss of membrane integrity (white bars) and analyzed by the FACS (Supplementary fig. 6). Values reflect the % of cells that shifted from normal to depolarized or to membrane permeable after subtracting background from untreated cells (n=5). **D.** Same assay as in C in the presence of inhibitors mitoquinone (MitoQ), Ebselen (Ebs), and trifluoroperazine (TFP) for 16 h (n=5). Inhibition was significant ($p<0.05$ by paired t-test) with all 3 inhibitors in *Fth*$^{\Delta/\Delta}$ cells both for depolarization and cell death, whereas in *Fth*$^{loxNeo/loxNeo}$ cells only depolarization was significantly inhibited by Ebselen and trifluoroperazine.

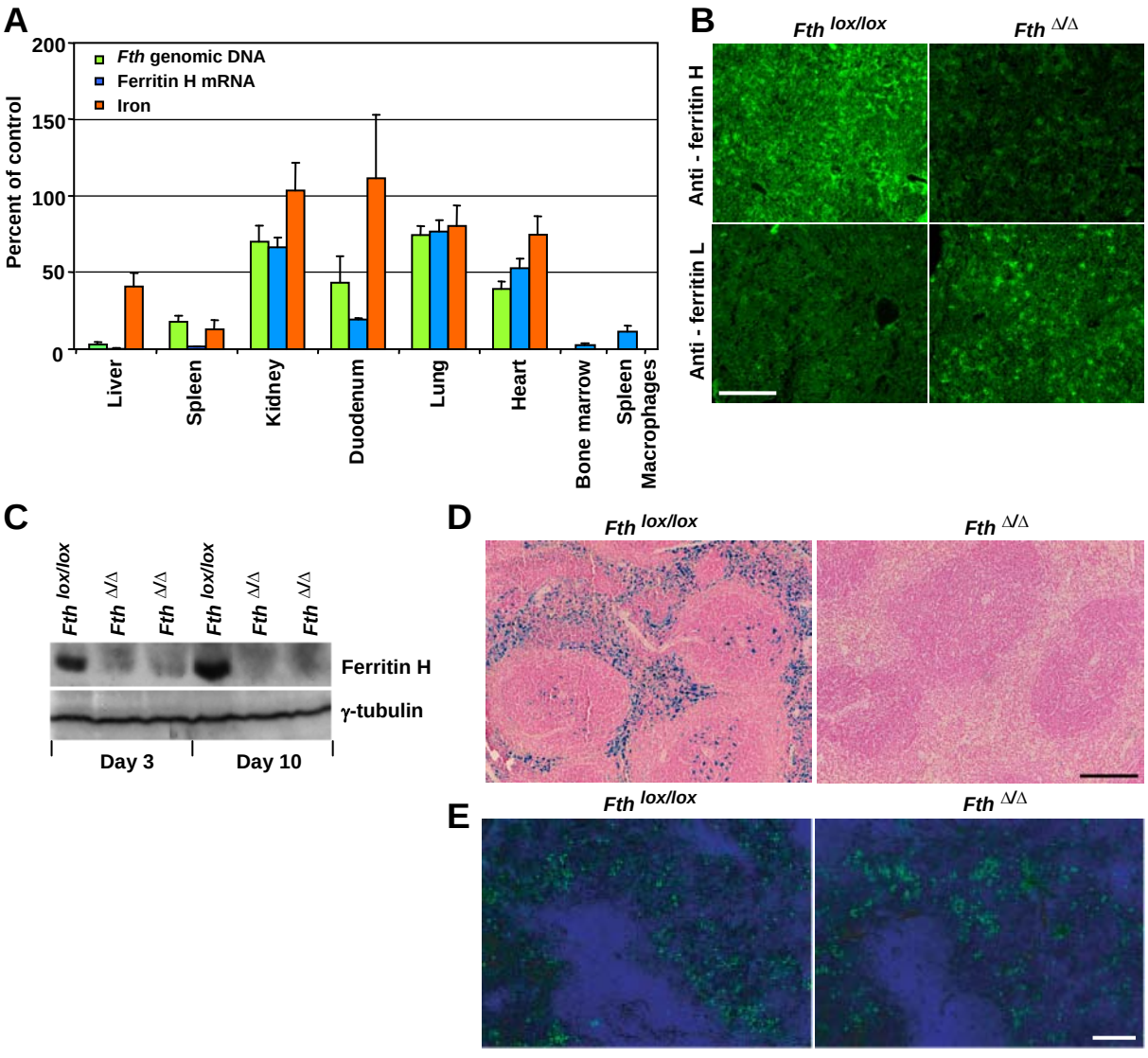
A
200
150
100
50
0
Percent of control
Fth genomic DNA
Ferritin H mRNA
Iron
Liver
Spleen
Kidney
Duodenum
Lung
Heart
Bone marrow
Spleen Macrophages
B
Fth lox/lox
Fth Δ/Δ
Anti - ferritin H
Anti - ferritin L
C
Fth lox/lox
Fth Δ/Δ
Fth Δ/Δ
Fth lox/lox
Fth Δ/Δ
Fth Δ/Δ
Ferritin H
γ-tubulin
Day 3
Day 10
D
Fth lox/lox
Fth Δ/Δ
E
Fth lox/lox
Fth Δ/Δ

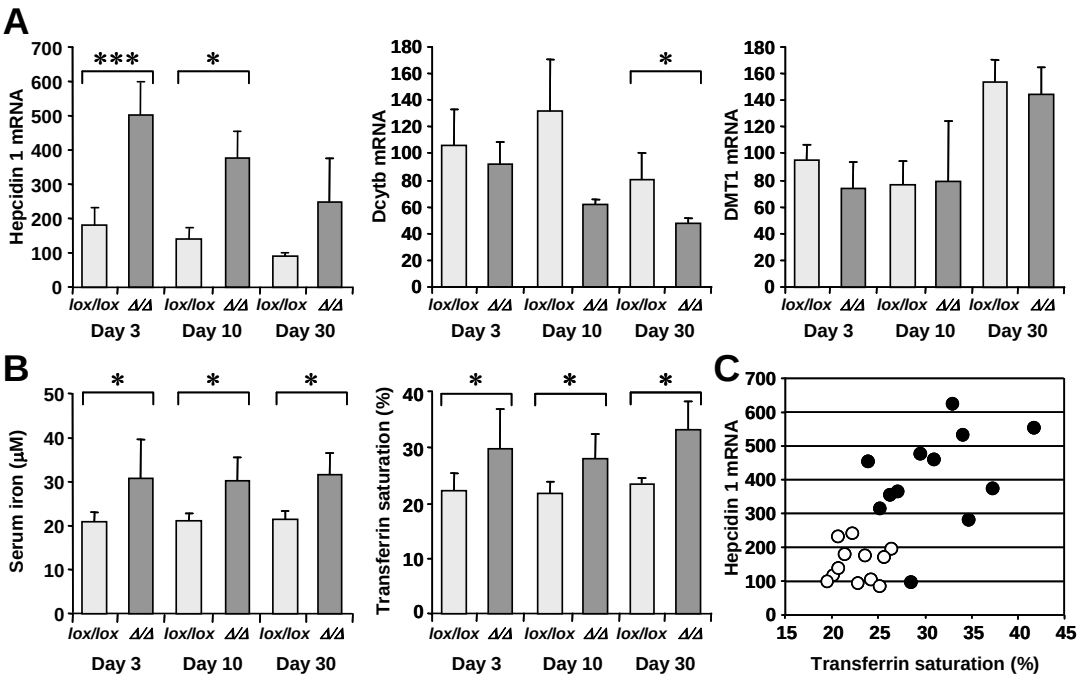
A
Hepcidin 1 mRNA
Dcytb mRNA
DMT1 mRNA
lox/lox
Δ/Δ
Day 3
Day 10
Day 30
B
Serum iron (μM)
Transferrin saturation (%)
C
Hepcidin 1 mRNA
Transferrin saturation (%)

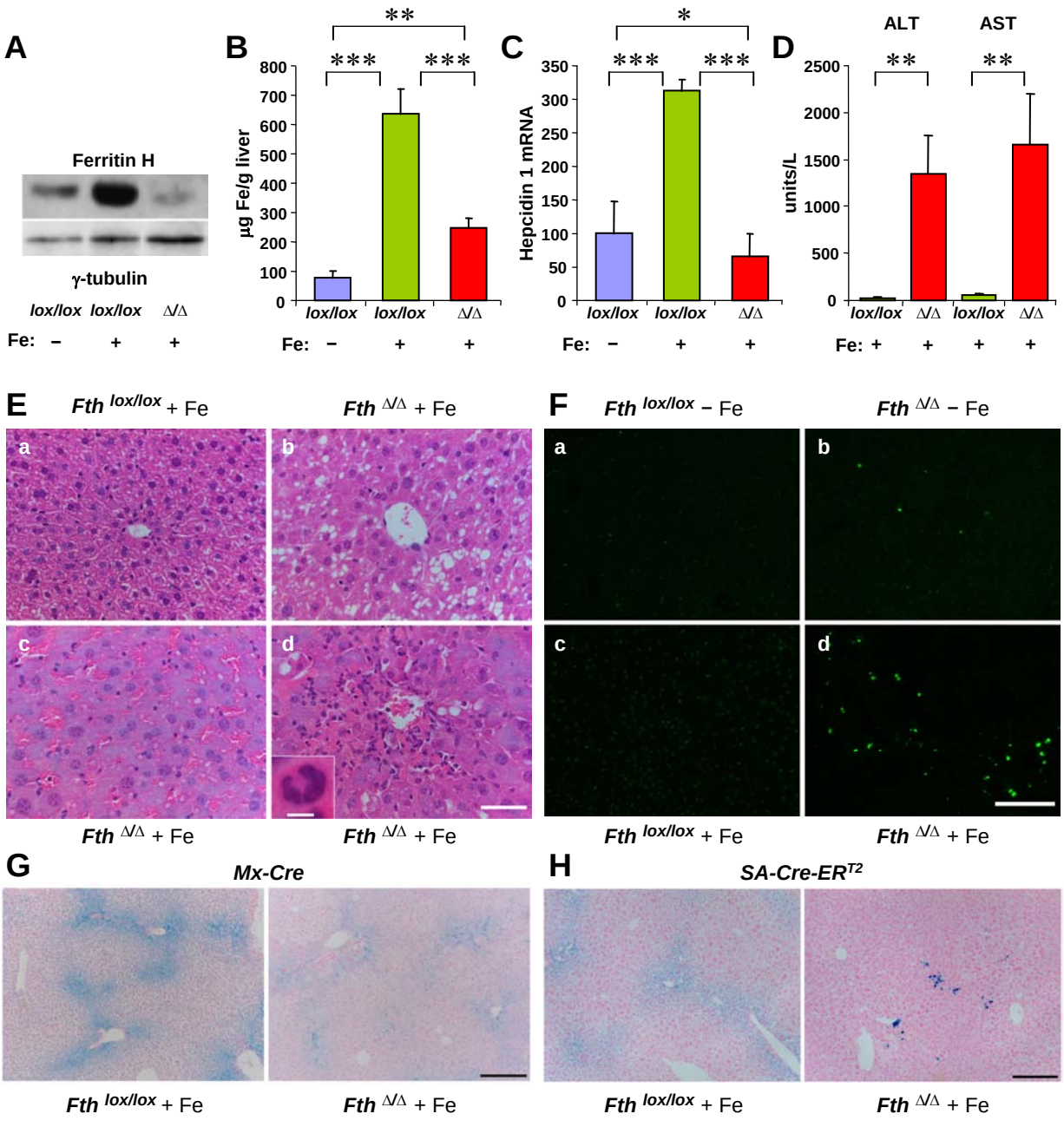
A
Ferritin H
γ-tubulin
lox/lox lox/lox Δ/Δ
Fe: – + +
B
µg Fe/g liver
800
700
600
500
400
300
200
100
0
**
***
***
lox/lox lox/lox Δ/Δ
Fe: – + +
C
Hepcidin 1 mRNA
350
300
250
200
150
100
50
0
*
***
***
lox/lox lox/lox Δ/Δ
Fe: – + +
D
ALT
AST
units/L
2500
2000
1500
1000
500
0
**
**
lox/lox Δ/Δ lox/lox Δ/Δ
Fe: + + + +
E
Fth lox/lox + Fe
Fth Δ/Δ + Fe
a
b
c
d
Fth Δ/Δ + Fe
Fth Δ/Δ + Fe
F
Fth lox/lox – Fe
Fth Δ/Δ – Fe
a
b
c
d
Fth lox/lox + Fe
Fth Δ/Δ + Fe
G
Mx-Cre
Fth lox/lox + Fe
Fth Δ/Δ + Fe
H
SA-Cre-ERT2
Fth lox/lox + Fe
Fth Δ/Δ + Fe

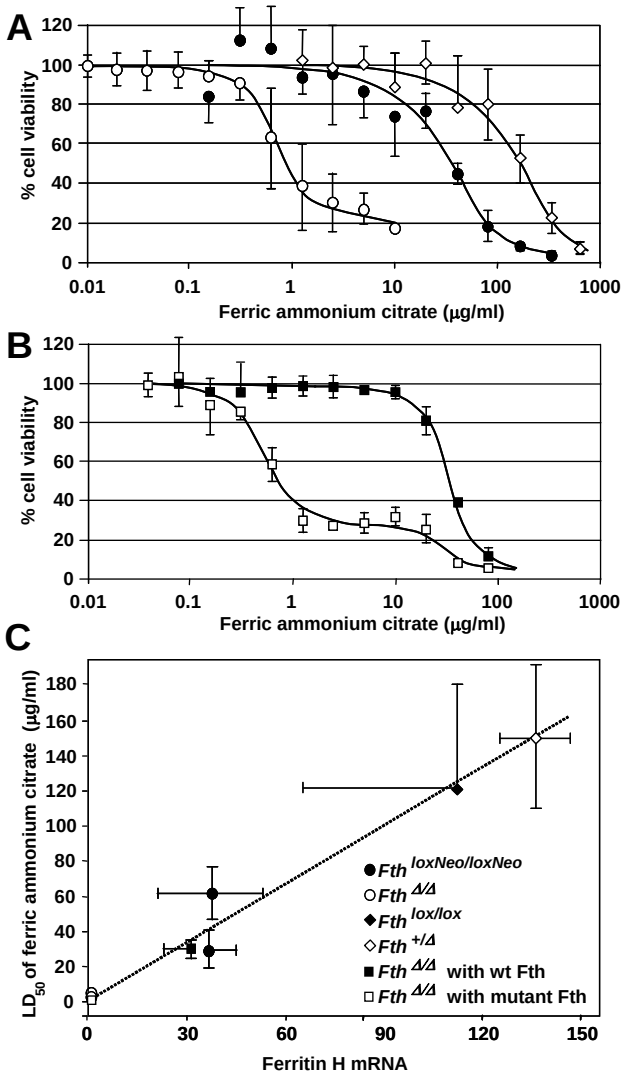
A
% cell viability
120
100
80
60
40
20
0
0.01
0.1
1
10
100
1000
Ferric ammonium citrate (μg/ml)
B
% cell viability
120
100
80
60
40
20
0
0.01
0.1
1
10
100
1000
Ferric ammonium citrate (μg/ml)
C
LD50 of ferric ammonium citrate (μg/ml)
180
160
140
120
100
80
60
40
20
0
0
30
60
90
120
150
Ferritin H mRNA
Fth loxNeo/loxNeo
Fth Δ/Δ
Fth lox/lox
Fth +/Δ
Fth Δ/Δ with wt Fth
Fth Δ/Δ with mutant Fth

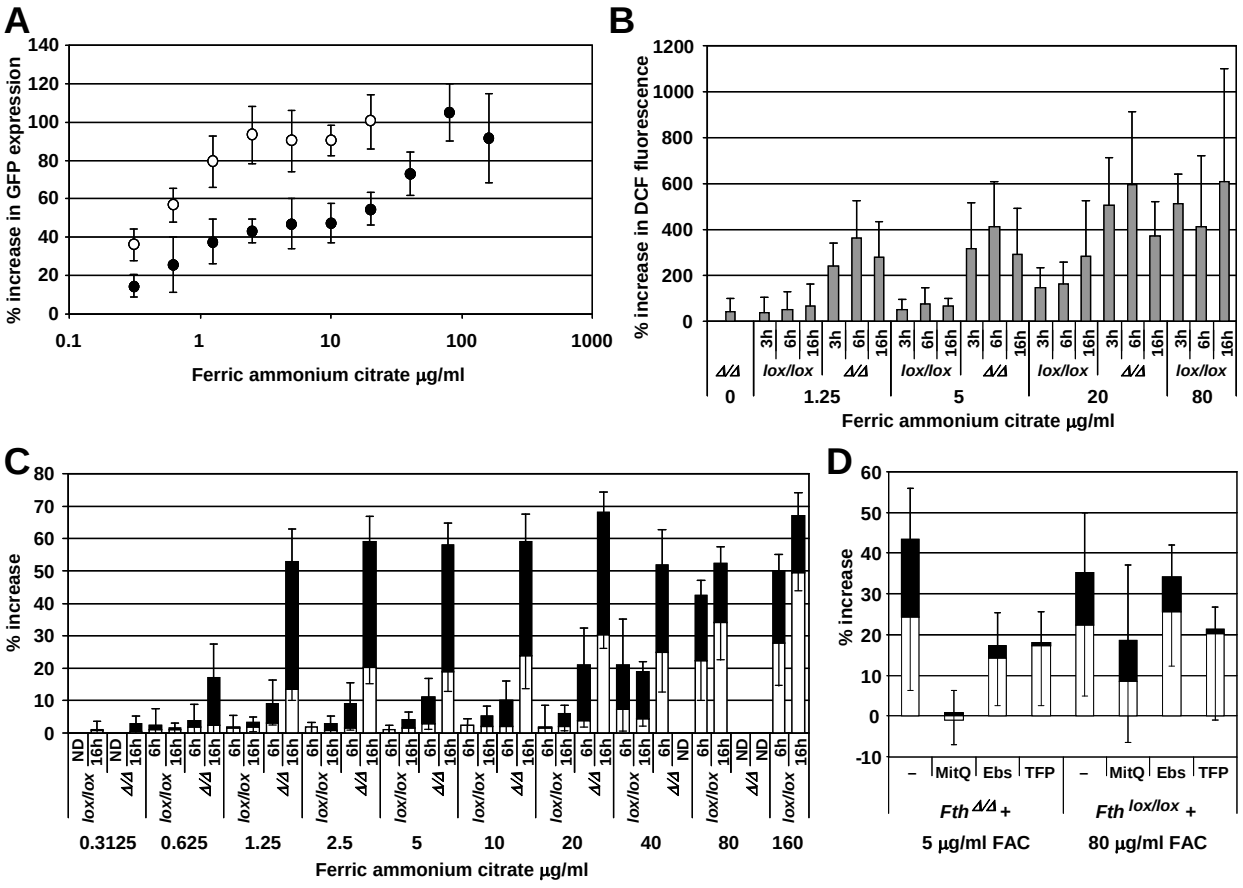
A
% increase in GFP expression
Ferric ammonium citrate µg/ml
B
% increase in DCF fluorescence
Δ/Δ
lox/lox
Ferric ammonium citrate µg/ml
C
% increase
Ferric ammonium citrate µg/ml
D
% increase
MitQ
Ebs
TFP
5 µg/ml FAC
80 µg/ml FAC

Supplementary Materials and Methods

Generation and analysis of mutant mice. All work with mice was carried out in conformity with Swiss legal obligations of authorization for animal experimentation. To generate the *Fth*^{loxNeo} allele we amplified genomic DNA from BAC clone 409B1 of the RP-22 BAC library acquired from Children's Hospital Oakland Research Institute. The 5' homologous arm (1.5 kb), a deletion region (677 bp) containing 386 bp of the 5' flanking promoter and exon 1 of the ferritin H gene, and 3' homologous arm (2.5 kb) were cloned into vector tvFS1, a derivative of TNLOX1-3 into which a FRT/loxPneo cassette was inserted.[1] The deletion region was flanked by *lox*P sites. The neomycin-resistance (Neo) cassette, flanked by two FRT sites, was used to select positive ES cell clones (Supplementary fig. 1A). Homologous recombinants in ES 129/Sv cells were identified first by PCR using primers in the Neo cassette and genomic upstream region as well as primers gFth1 and 2 (for primers see Supplementary table 2). Of 200 neomycin-resistant ES cell clones, 6 showed the correct arrangement for a recombination event. They were confirmed by genomic Southern blot analysis of an *Eco*RI digest with an intron 1 specific probe (Supplementary fig. 1B). Mutant ES cells were introduced into blastocysts of C57BL/6 mice to generate chimeras that transmitted the *Fth*^{loxNeo} allele through the germ-line. Mice carrying the *Fth*^{loxNeo} allele were genotyped by PCR (Supplementary fig. 1C). Primers used were gFth1 and 2 to detect the wildtype (419 bp) and floxed allele (337 bp). Subsequent to the exon 1 deletion by Cre recombinase, the *Fth*$^{-}$ allele was genotyped with primers gFth1 and 3, and gave a band of 530 bp (Supplementary fig. 1C). For initial experiments, mice with the *Fth*^{loxNeo} allele were on a mixed genetic background (C57BL/6 x 129/Sv) and crossed with nestin-Cre transgenic mice[2] to obtain *Fth*$^{loxNeo/+}$*;Nes-Cre1* mice. Mice were genotyped for Cre by PCR. The *Fth*^{lox} allele was generated by crossing mice carrying the *Fth*^{loxNeo} allele to transgenic mice with β-actin-FlpE recombinase.[3] Mice with the *Fth*^{lox} allele on mixed genetic background (C57 BL/6 x 129/Sv) were crossed with the Mx-Cre transgenic mice[4] to obtain *Fth*$^{lox/lox}$*;Mx-Cre* (mutant) and *Fth*$^{lox/lox}$*;+* (control) mice. Upon advancement of the analysis, mice were 10 times backcrossed with C57BL/6J mice purchased from Harlan (Harlan, Bicester, UK). For initial experiments, the ferritin H deletion was induced by 3 intraperitoneal injections of poly-IC (Sigma, St. Louis, MO) at 100 mg/kg. In later experiments we switched to a more active source of poly-IC (InvivoGen, San Diego, CA). For liver deletion experiments, 1 mg/kg body weight was injected 2 times, every third day. For experiments to study deletion in the bone marrow, spleen and thymus, it was sufficient to inject mice 5 times with poly-IC (InvivoGen,

San Diego, CA) at 0.1 mg/kg body weight, every other day. All control mice were littermates of mutant mice and were injected with poly-IC. *Fth*$^{lox/lox}$;*SA-Cre-ER*^{T2} mice generated by breeding with *SA-Cre-ER*^{T2} mice.[5] The hepatocyte-specific ferritin H gene deletion was induced with 100 μl tamoxifen (1 mg/ml)(Sigma) on 5 consecutive days. Where indicated poly-IC was injected together with tamoxifen on days 1 and 4.

Mice were fed with food at a normal iron content of 200 mg/kg. Where indicated mice received powdered food supplemented with 25g/kg carbonyl iron for 14 days before and during the experiment.

Plasmid constructs. To obtain pKI-MerCreMer, Cre-ER^{T} in pKI-Cre-ER^{T} (gift of Andreas Trumpp) was replaced with MerCreMer from pAN-MerCreMer (gift of Michael Reth). To obtain pSH-FTL-d2EGFP, the SV40 promoter-Hygromycin cassette from pBabe-Hygro and a cassette containing a CMV promoter and d2EGFP (Clontech, Mountain View, CA) were first inserted in opposite orientation into the backbone from the vector ZPCTHG.[6] Next the 5'UTR of mouse ferritin L cDNA (bases 6-209 of NCBI #AK169159) was amplified by PCR, inserted at the N-terminus of d2EGFP. To obtain ferritin H expression vectors for the wildtype and mutant (62E→K;65H→G), myc-AUF1 in SLHGC-MYCAUF[6] was replaced with a PCR amplified Fth cDNA (BC012314).

Mouse embryonic fibroblasts. Cells were derived from *Fth*$^{loxNeo/loxNeo}$ and *Fth*$^{loxNeo/+}$ mice using a standard protocol. Cells were cultured in DMEM-10% FCS. Initially *Fth*$^{loxNeo/loxNeo}$ was transformed with pKI-Cre-ER^{T} to obtain *Fth*$^{\Delta/\Delta}$. However, following selection with 2 μg/ml puromycin, the deletion occurred spontaneously in absence of tamoxifen treatment in 96% of the cells. The *Fth*$^{\Delta/\Delta}$ and *Fth*$^{+/\Delta}$ cells generated this way were used only for LD_{50} determinations and for Fth overexpression by transformation with both pBSWITCH and SLHGCG-FtH or FtH mutant.[6] A *Fth*$^{lox/lox}$ cell line was generated by subcloning of *Fth*$^{loxNeo/loxNeo}$ cells transfected with pOG44 (Invitrogen, Carlsbad, CA), which expresses Flip recombinase. Subsequently we generated a cell line that does not delete ferritin H spontaneously. For this, *Fth*$^{loxNeo/loxNeo}$ cells were infected with pKI-MerCreMer retrovirus and selected on 2 μg /ml puromycin. A clone permissive for deletion with 1 μM 4-OH tamoxifen was transformed with the retrovirus pSH-FTL-d2EGFP. Following selection with 200 μg/ml hygromycin, the cell population was tested for ferric ammonium citrate- and desferrioxamine-regulated d2EGFP expression. Cells were sorted with a FACSAria (Becton Dickinson,

Franklin Lakes, NJ) for high and intermediate levels of GFP expression. The sorted cells (FTL-GFP) were used for all cell culture of iron toxicity tests.

FACS analysis of iron toxicity. To assess cell viability, the cell titer non-radioactive cell proliferation assay was used (Promega, Madison, WI). To test mitochondrial depolarization and cell membrane integrity, cells were trypsinized and stained in DMEM at 37°C for 10 min with 250 nM tetramethyl rhodamine methyl ester (TMRM) (Sigma) and 2 μg/ml 7-amino-actinomycin D (7aaD) (Sigma). At least 10,000 events were acquired with a FACScan (Becton Dickinson) using channels 1, 2, and 3 for GFP, TMRM, and 7aaD respectively. The % increase in mean GFP fluorescence was measured in a window of coloured cells (Supplementary fig. 3). To measure ROS, cells were washed in Hepes-buffered saline and stained 30 min at 37°C with 10 μM 2',7'-dichlorodihydrofluorescein diacetate (H2DCFDA) (Molecular Probes, Eugene, OR) followed by propidium iodide (PI) (Sigma). The dichlorofluorescein (DCF) product was measured in channel 1 and PI in channel 3 for at least 3,000 cells. ROS activity was calculated from DCF as the % increase in mean fluorescence above untreated control cells. Cell Quest was used for analysis. To measure mitochondrial permeability transition (MPT), cells were incubated with 1 μM calcein AM (Biotium, Hayward CA) and 1 mM cobalt chloride (Sigma) in conjunction with TMRM and 7aaD prior to FACS analysis.[7, 8] The fluorescent calcein product of calcein AM hydrolysis was read in FACScan channel 1 and analysed with FloJoe. Mitoquinone[9] (0.5 μM) (gift of Michael Murphy), 20 μM Ebselen[10] (Sigma), 5 μM trifluoroperazine (Sigma) or 4 μM cyclosporin A were added as inhibitors together with iron salt.

Real-time PCR assays. Deletion of the ferritin H gene in *Fth*$^{lox/lox}$*;Mx-Cre* mutant mice was assessed by real-time PCR on genomic DNA prepared by DNAeasy kit (Qiagen, Hilden, Germany) and on cDNA prepared from total RNA (RNAeasy kit, Qiagen). Real-time PCR assay was performed using LightCycler (Roche Diagnostics, Rotkreuz, Switzerland) either with dual labeled probe (FAM/TAMRA) or with SYBR green dye. For a detailed list of primers see Supplementary table 2. PCR measurements of genomic DNA were normalized to the 18S rRNA gene, ferritin H cDNA to of mouse acidic ribosomal phosphoprotein P0 cDNA or TATA box binding protein cDNA, and cDNAs of all other genes to GAPDH, HPRT and β-actin cDNA.

Biochemical assays. Tissue iron was determined by the bathophenanthroline method on acid-solubilized wet tissue.[11] Hematocrit was determined by standard procedures. Hemoglobin was measured by the cyanmethemoglobin method (Sigma). Serum iron and total iron binding capacity were measured with the Diagnostic Chemicals kit (DCL, Charlottetown, Canada). Alanine transaminase (ALT; GPT; EC 2.6.1.2) and aspartate transaminase (AST; GOT; EC 2.6.1.1) activity was measured in serum using Stanbio reagents (Stanbio, Boerne, TX).

Immunoblotting. Liver (100 mg) was homogenized in 1 ml hypotonic extraction buffer (25 mM HEPES, pH 7.5, 5 mM $MgCl_2$, 1 mM EGTA) with a protease inhibitor cocktail (Complete Mini, Roche) and centrifuged at 15,000x*g* for 15 min. Protein of the supernatant (100 μg/sample) was separated by SDS-polyacrylamide gel electrophoresis and transferred to Optitran BA-S 83 cellulose nitrate membranes (Schleicher & Schuell BioScience, Dassel, Germany) for ferritin, or Hybond nitrocellulose membranes (Amersham, Buckinghamshire, UK) for tubulin. Membranes were blocked with 5% non-fat dry milk (1 h) in TBST buffer (100 mM Tris-HCl, pH 7.8, 150 mM NaCl, 0.1% Tween-20), and then incubated with rabbit anti-ferritin H chain antibody H-53 (1:1,000, Santa Cruz Biotechnology, Santa Cruz, CA), or monoclonal anti-γ-tubulin antibody (T6557, 1:5,000, Sigma) at 4^{o}C, overnight. HRP-conjugated secondary antibody (2 h, 25^{o}C), enhanced chemiluminescence reagent, and SuperRX (Fujifilm, Tokyo, Japan) were used to visualize immuno-reactive proteins.

Macrophage isolation. Splenic macrophages were enriched by centrifugation for 30 min at 4^{o}C on an iso-osmotic Percoll (Pharmacia, Uppsala, Sweden) step gradient.[12]

Histology and immunofluorescence microscopy. Iron stores in ferritin were histochemically visualized by the Perl's Prussian blue staining. Hematoxylin-eosin staining was done with a standard protocol. The terminal transferase dUTP nick end labelling (TUNEL) assay was done on paraffin embedded sections with the *in situ* Cell Death Detection Kit (Roche). For immunofluorescence microscopy, dissected tissues were embedded in OCT (Sakura Finetek, Torrance, CA) without prior fixation. Cryostat sections (8 μm) on Superfrost/Plus glass slides (Thermo Fisher Scientifi**c,** Waltham, MA**)** were air-dried overnight, and then fixed in ice-cold acetone for 10 min. After rehydration, sections were blocked using 0.1% bovine serum albumin (BSA) and 1–4% normal mouse serum (NMS). Ferritin H and L were visualized using specific rabbit antibodies H53 and H45 (Santa Cruz Biotech, Santa Cruz, CA),

respectively, and FITC-labeled anti-rabbit IgG. To stain most macrophage populations rat anti-CD11b and rat anti-F4/80 antibodies were combined (diluted in PBS containing 0.1% BSA, 1% normal mouse serum) and detected using a goat-anti-rat biotinylated antibody followed by streptavidin Cy3 (Jackson ImmunoResearch, West Grove, PA).

Statistical methods. Data of experimental versus control mice were compared for the significance of changes by calculating p-values using Student's T test.

References for Supplementary Materials and Methods

1. Radtke F, Wilson A, Stark G, Bauer M, van Meerwijk J, MacDonald H, Aguet M. Deficient T cell fate specification in mice with an induced inactivation of Notch1. Immunity 1999;10:547-558.
2. Trumpp A, Depew MJ, Rubenstein JL, Bishop JM, Martin GR. Cre-mediated gene inactivation demonstrates that FGF8 is required for cell survival and patterning of the first branchial arch. Genes Dev. 1999;13:3136-3148.
3. Dymecki SM. Flp recombinase promotes site-specific DNA recombination in embryonic stem cells and transgenic mice. Proc. Natl Acad. Sci. USA 1996;93:6191-6196.
4. Kühn R, Schwenk F, Aguet M, Rajewsky K. Inducible gene targeting in mice. Science 1995;269:1427-1429.
5. Schuler M, Dierich A, Chambon P, Metzger D. Efficient temporally controlled targeted somatic mutagenesis in hepatocytes of the mouse. Genesis 2004;39:167-172.
6. Paschoud S, Dogar AM, Kuntz C, Grisoni-Neupert B, Richman L, Kühn LC. Destabilization of interleukin-6 mRNA requires a putative RNA stem-loop structure, an AU-rich element and the RNA-binding protein AUF1. Mol. Cell. Biol. 2006;26:8228-8241.
7. Petronilli V, Miotto G, Canton M, Brini M, Colonna R, Bernardi P, Di Lisa F. Transient and long-lasting openings of the mitochondrial permeability transition pore can be monitored directly in intact cells by changes in mitochondrial calcein fluorescence. Biophys. J. 1999;76:725-734.
8. Poncet D, Boya P, Metivier D, Zamzami N, Kroemer G. Cytofluorometric quantitation of apoptosis-driven inner mitochondrial membrane permeabilization. Apoptosis 2003;8:521-530.
9. Kelso GF, Porteous CM, Coulter CV, Hughes G, Porteous WK, Ledgerwood EC, Smith RAJ, et al. Selective targeting of a redox-active ubiquinone to mitochondria within cells. Antioxidant and antiapoptotic properties. J. Biol. Chem. 2001;276:4588-4596.
10. Müller A, Cadenas E, Graf P, H. S. A novel biologically active seleno-organic compound - I. Glutathione peroxidase-like activity *in vitro* and antioxidant capacity of PZ 51 (Ebselen). Biochem. Pharmacol. 1984;33:3235-3239.
11. Torrance JD, Bothwell TH. Tissue iron stores. Methods Hematol. 1980;1:90-115.
12. Plasman N, Vray B. Mouse peritoneal macrophages: characterization of functional subsets following Percoll density gradients. Res. Immunol. 1993;144:151-163.

Supplementary Table 1. Hematological parameters

	10 days		30 days		120 days	
	Fth $^{lox/lox}$	***Fth*** $^{\Delta/\Delta}$	***Fth*** $^{lox/lox}$	***Fth*** $^{\Delta/\Delta}$	***Fth*** $^{lox/lox}$	***Fth*** $^{\Delta/\Delta}$
Hemoglobin (g/dl)	17.5 ± 2.0	17.2 ± 0.8	21.5 ± 1.3	20.8 ± 0.6	22.1 ± 1.6	21.8 ± 1.6
Hematocrit (%)	40.7 ± 1.6	38.1 ± 0.6	43.4 ± 4.4	41.5 ± 2.8	44.6 ± 1.4	44.7 ± 4.2

n=4 in each group

Supplementary Table 2. Primers used for RT-PCR and PCR measurements.

Gene	Primer name	Sequence	Accession Nr	Amplicon
Genotyping				
Ferritin H, genomic	gFth2 forward in exon1	CCATCAACCGCCAGATCAAC	NC_000085	lox 337
	gFth1 reverse in intron1	CGCCATACTCCAGGAGGAAC		wt 420
	gFth3 in promoter	GGCTGTTGTCCTGCTCTAAG		del 520
Cre	Cre forward	GCCAGGCGTTTTCTGAGCATAC	X03453	884
	Cre reverse	CACCATTGCCCCTGTTTCACTATC		
LightCycler/Sybr				
Hepcidin 1	Hamp1 forward	AGAGCTGCAGCCTTTGCAC	NM_032541	130
	Hamp1 reverse	ACACTGGGAATTGTTACAGCATTTA		
DMT1/NRAMP2	DMT1 forward	GCAGTGGTTAGCGTGGCTTATT	NM_008732	74
	DMT1 reverse	AGACAGACCCAATGCAATCAAA		
Ferroportin/IREG	IREG forward	TTGCAGGAGTCATTGCTGCTA	NM_016917	101
	IREG reverse	TGGAGTTCTGCACACCATTGAT		
Dcytb	Dcytb forward	GCAGCGGGCTCGAGTTTA	NM_028593	98
	Dcytb reverse	TTCCAGGTCCATGGCAGTCT		
Hephaestin	Heph forward	TTGTCTCATGAAGAACATTACAGCAC	NM_010417	160
	Heph reverse	CATATGGCAATCAAAGCAGAAGA		
Hfe	Hfe forward	CTGGGACAGCAAGTGCCTACT	NM_010424	83
	Hfe reverse	TCCAGAGCCTGACACCTTAGAGA		
Tf receptor 1	TfR1 forward	GTTTTTGTGAGGATGCAGACTATCC	NM_011638	81
	TfR1 reverse	GCTGAGGAACTTTCTGAGTCAATG		
Tf receptor 2	TfR2 forward	GCCATGTTTCTCCGGTTCCT	NM_015799	133
	TfR2 reverse	GGCGCGAGAGCTTATCGA		
Transferrin	Tf forward	CCATCCCATCACAACAAGGTATC	NM_133977	74
	Tf reverse	GCTAGTGTCCGATGCCTTCAC		
Glutathione per-oxidase 1	Gpx1 forward	GCGGCCCTGGCATTG	NM_008160	132
	Gpx1 reverse	GGACCAGCGCCCATCTG		
Superoxide dismutase 2	Sod2 forward	CACATTAACGCGCAGATCATG	NM_013671	100
	Sod2 reverse	CCAGAGCCTCGTGGTACTTCTC		
Heme-oxygenase 1	HO1 forward	GCCACCAAGGAGGTACACAT	NM_010442	132
	HO1 reverse	GCTTGTTGCGCTCTATCTCC		
HPRT1	Hprt1 forward	CCTAAGATGAGCGCAAGTTGAA	NM_013556	86
	Hprt1 reverse	CCACAGGACTAGAACACCTGCTAA		
GAPDH	GAPDH forward	AATGTGTCCGTCGTGGATCTGA	NM_008084	83
	GAPDH reverse	GATGCCTGCTTCACCACCTTCT		
Actin β	Act β forward	GACAGGATGCAGAAGGAGATTACTG	NM_007393	124
	Act β reverse	GCTGATCCACATCTGCTGGAA		
TATA box binding protein	Tbp forward	CCCCTTGTACCCTTCACCAAT	NM_013684	89
	Tbp reverse	GAAGCTGCGGTACAATTCCAG		
LightCycler/TaqMan Primers and Probes				
Ferritin H, mRNA	mFeH forward	CCATCAACCGCCAGATCAAC	NM_010239	85
	mFeH reverse	GCCACATCATCTCGGTCAAA		
	mFeH Probe	AGTTGTATGCCTCCTACGTCTATCTGTCTATGTCTTGTT		
Mouse acidic ribosomal protein P0	mArbp P0 forward	CTTTGGGCATCACCACGAA	NM_007475	92
	mArbp P0 reverse	GCTGGCTCCCACCTTGTCT		
	mArbp P0 probe	ATCAGCTGCACATCACTCAGAATTTCAATGGT		

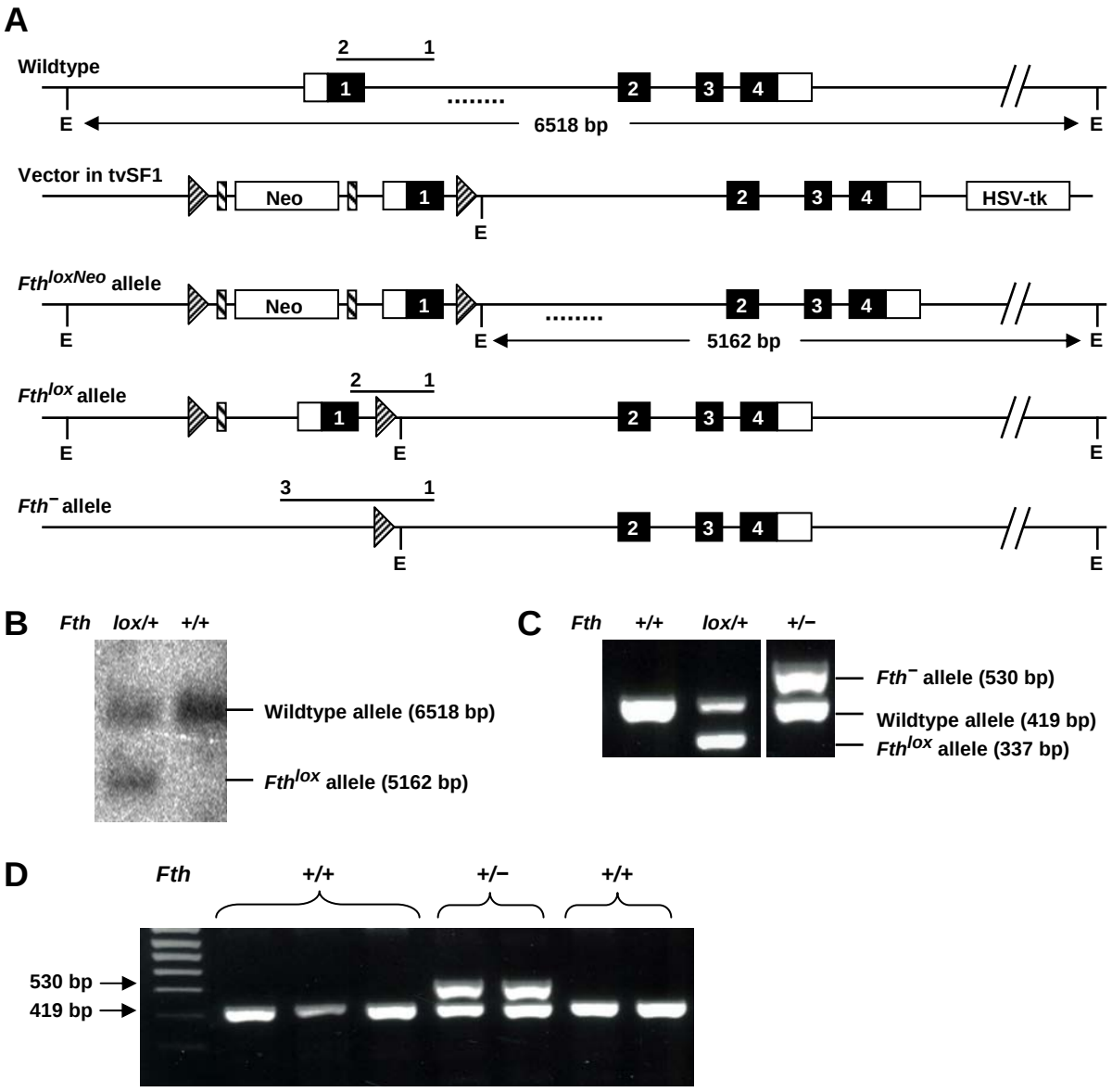

Supplementary figure 1. Targeting the mouse ferritin H gene with loxP and FRT sites. A. Steps in the conditional ferritin H deletion are described in detail in *Experimental procedures*. The targeting vector comprised the ferritin H promoter and exon 1 between *loxP* sites (hatched triangles), 1.5 kb of 5' and 2.5 kb of 3' flanking sequences. A neomycin selection cassette (Neo) flanked by FRT sites (hatched bars) was used for the selection of homologous recombination in ES cells. **B.** The recombination in ES cells was verified by a genomic Southern blot using an intron 1 probe (dashed line). **C.** A recombined ES cell clone carrying the *Fth*^{loxNeo} allele was introduced into blastocysts to generate chimeras that transmitted the *Fth*^{loxNeo} through the germ-line. Mice carrying the *Fth*^{lox} allele without the Neo cassette were obtained by breeding with transgenic mice that express the Flip recombinase. For routine genotyping of the *Fth*^{loxNeo}, the *Fth*^{lox} and the *Fth*$^{-}$ allele, specific primer sets were used to amplify as indicated by the black bars. **D.** Four litters of *Fth*^{loxNeo}*;Nes-Cre1*x*Fthl*^{oxNeo}*;Nes-Cre1* crosses, as the one shown here, were analyzed by tail genotyping. No mice with a *Fth*$^{-/-}$ genotype were born.

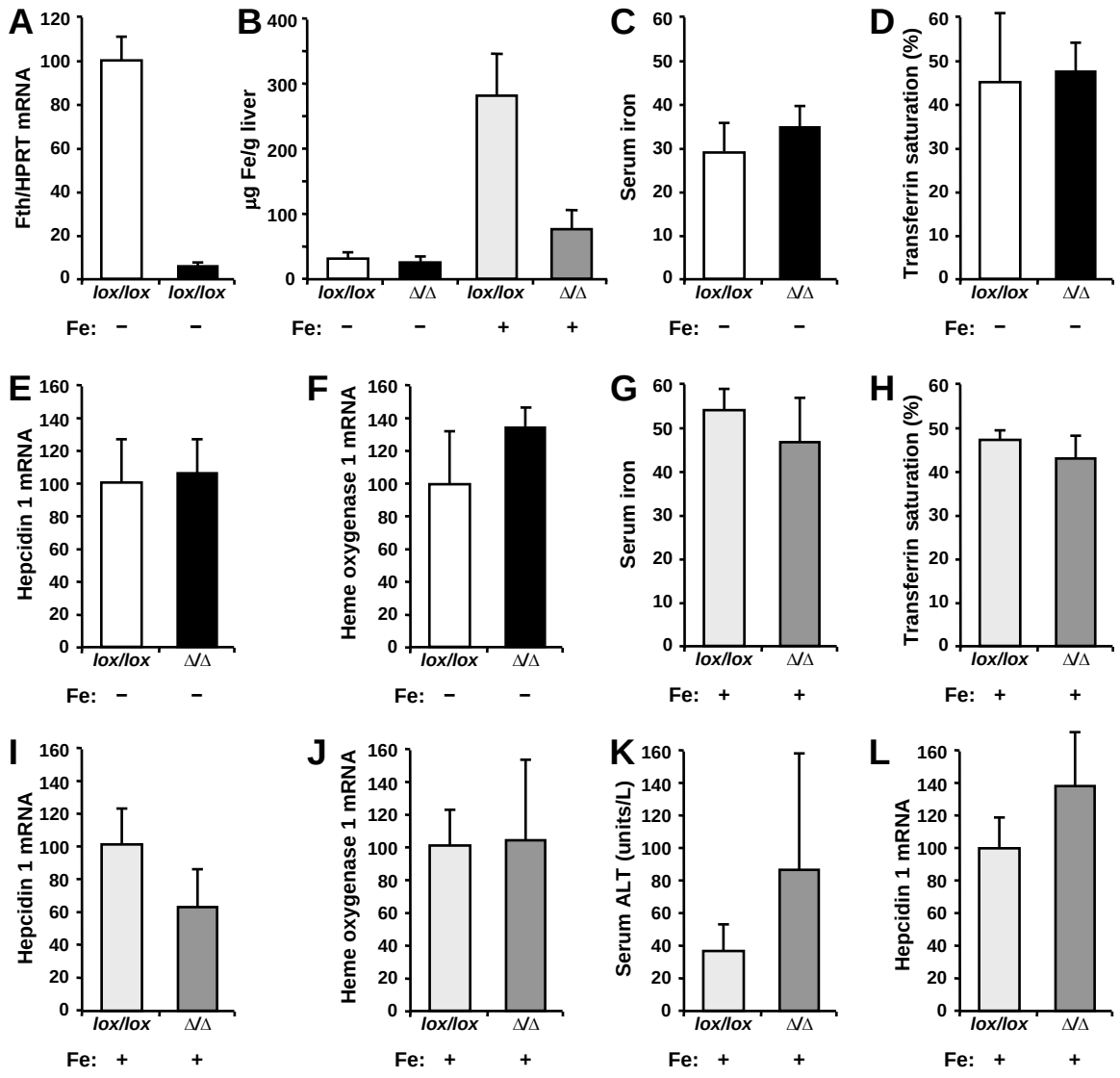

Supplementary figure 2. Analysis of *Fth*$^{lox/lox}$ and *Fth*$^{\Delta/\Delta}$ mice deleted with hepatocyte-specific SA-Cre-ER^{T2} and tamoxifen. For all experiments, 4 control *Fth*$^{lox/lox}$ and 4 deleted *Fth*$^{\Delta/\Delta}$ mice were analyzed at day 10, either under normal iron diet (–) or after a high-iron regimen (+). **A.** After deletion of the ferritin H gene, 6-15% liver ferritin H mRNA, normalized to HPRT mRNA, remained. **B.** Liver tissue iron prior and after ferritin H deletion. Under normal diet only about 15% of stored liver iron was lost. At high-iron regimen, liver iron accumulated 7-foldand was rapidly, but not completely lost from the tissue after ferritin H deletion. **C and D.** In normally fed mice, serum iron levels and transferrin saturation were slightly but not significantly increased after ferritin H deletion. **E and F.** Hepcidin 1 and heme oxygenase mRNA levels normalized to MTBP mRNA were not significantly change by the deletion. **G and H.** Serum iron levels and transferrin saturation were relatively high in control mice and not significantly changed after ferritin H deletion. If anything they were slightly diminished at day 10 after deletion. **I and J.** Hepcidin 1 and heme oxygenase 1 mRNA normalized to MTBP mRNA were not significantly changed in iron-loaded animals upon ferritin H deletion. **K.** Serum alanine transaminase (ALT) was only 2-fold increased by the ferritin H deletion indicating absence of tissue damage in these mice. **L.** Upon coinjection of poly-IC together with tamoxifen, hepcidin 1 mRNA was slightly, but not significantly induced.

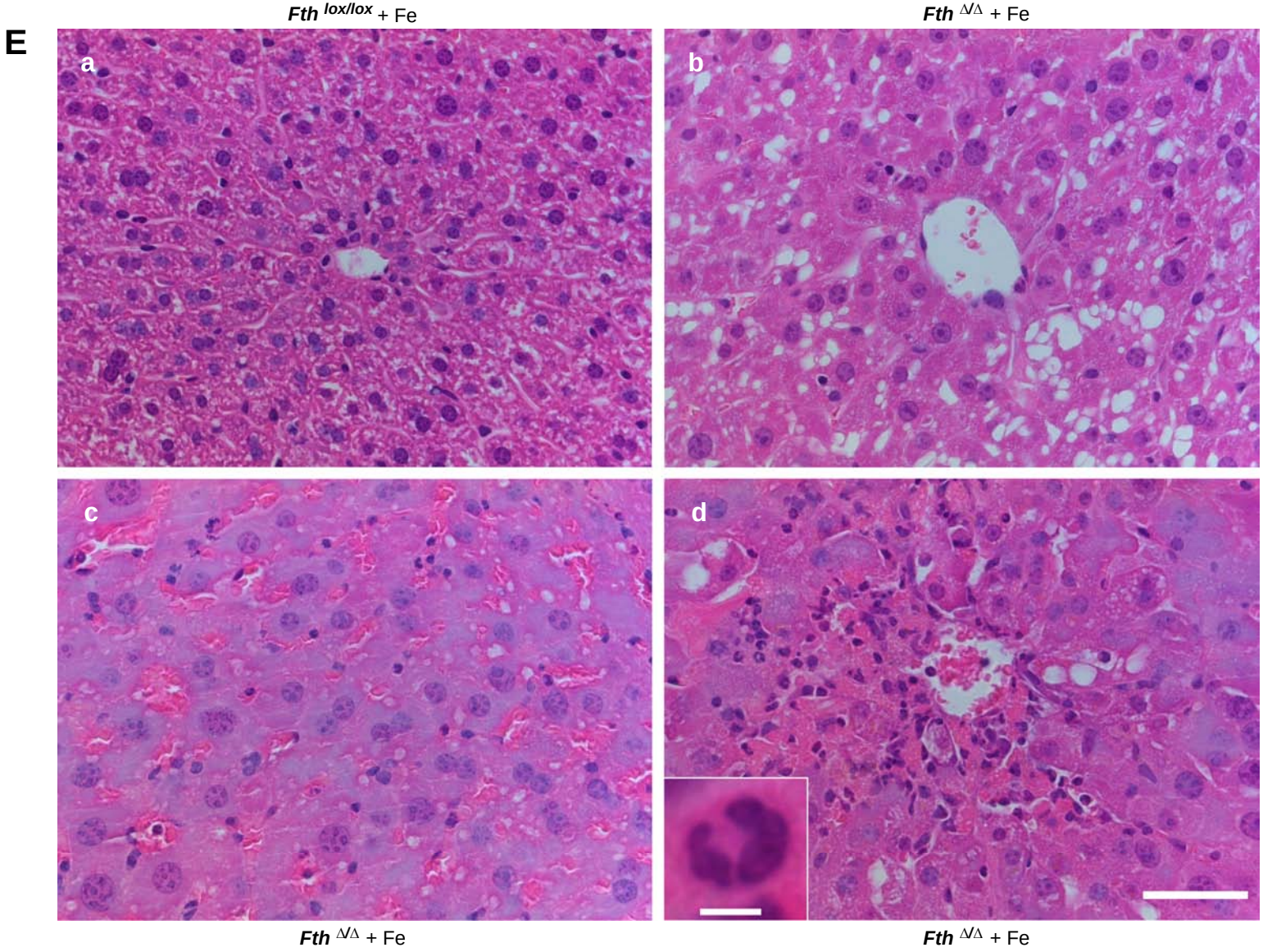

Supplementary figure 3. Enlarged version of Fig. 3 E.

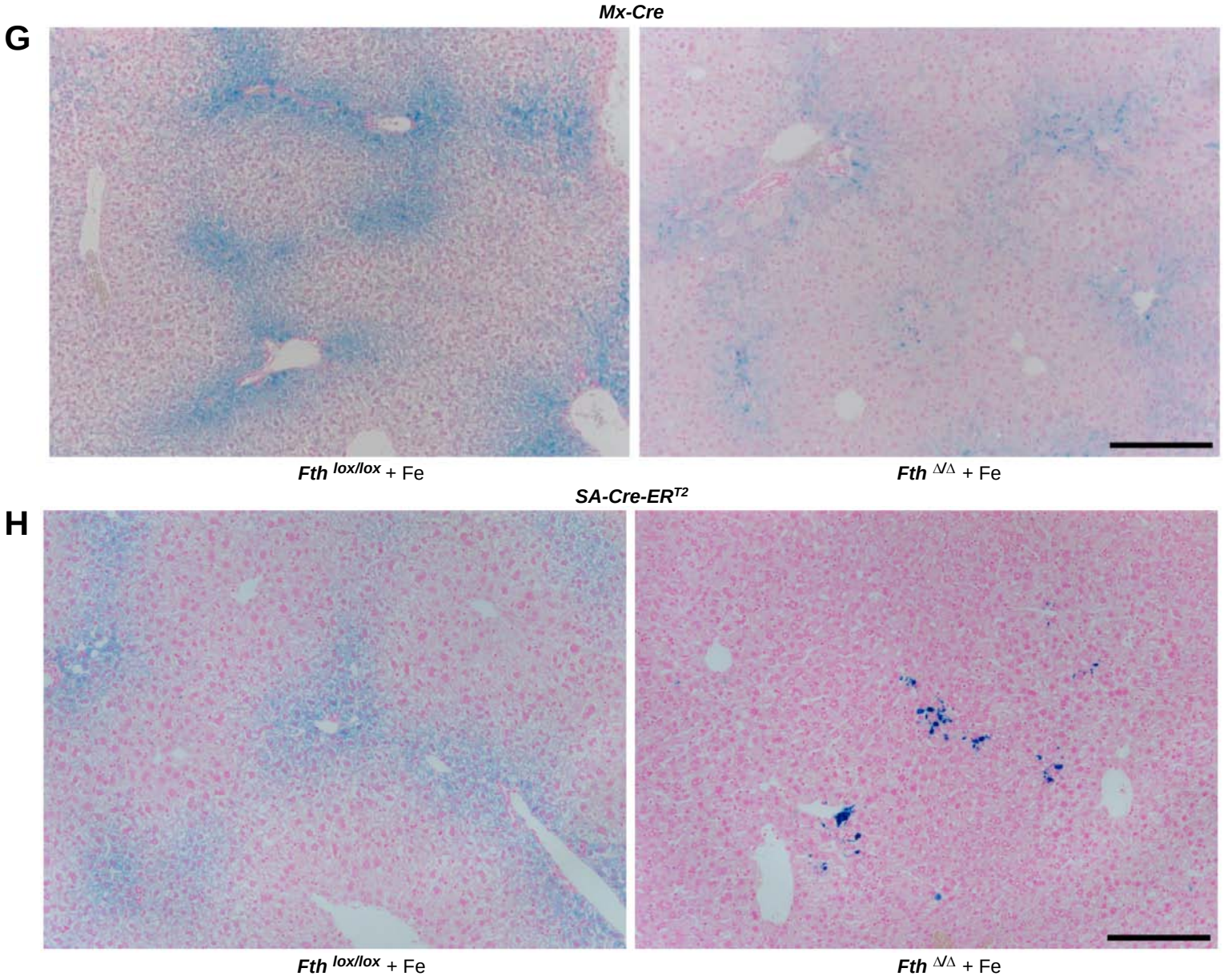

Supplementary figure 4. Enlarged version of Figs 3 G and H.

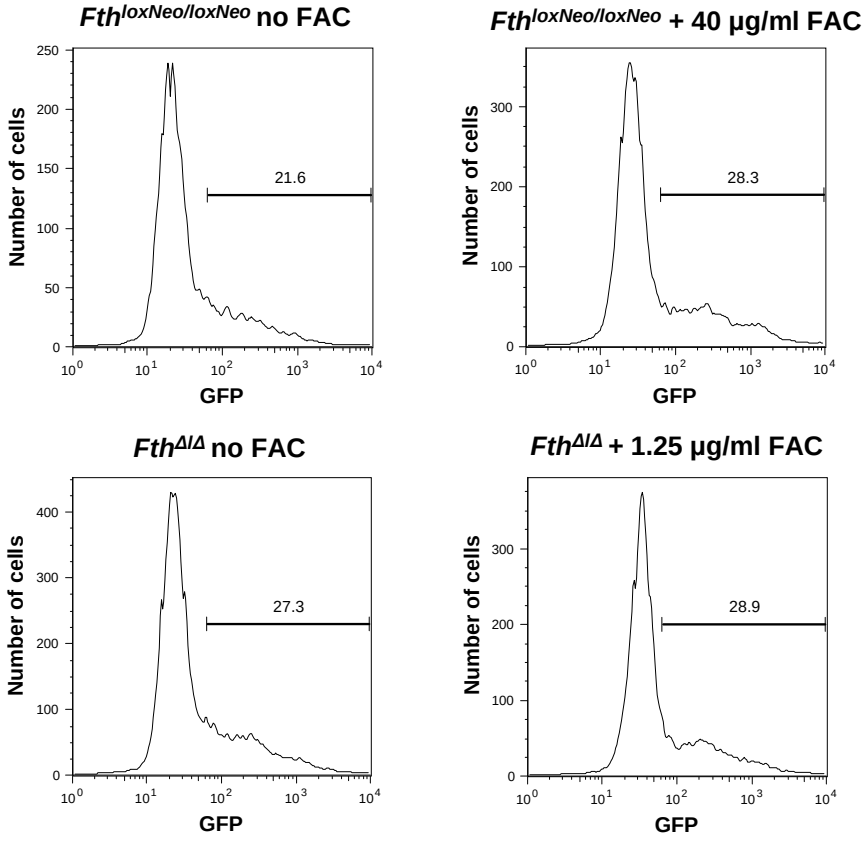

Supplementary figure 5. FACS profiles of d2EGFP expression in mouse embryonic fibroblasts. *Fth*$^{loxNeo/loxNeo}$ cells were stably infected with the retroviral vector pSH-FTL-d2EGFP to generate a cell population expressing unstable GFP under the translational control of iron regulatory proteins. Cells with high to intermediate GFP expression were selected with the FACS. *Fth*$^{\Delta/\Delta}$ cells were derived from this population by Cre-mediated gene deletion. These cells were then exposed to increasing amounts of ferric ammonium citrate (FAC). The mean fluorescence measured without FAC was 11.7% higher in *Fth*$^{\Delta/\Delta}$ cells than *Fth*$^{loxNeo/loxNeo}$ cells. This was significant ($p<0.005$; $n=10$). The increase of mean fluorescence after addition of FAC was compared to the one before addition and expressed as % increase. The data are reported in Figure 5A.

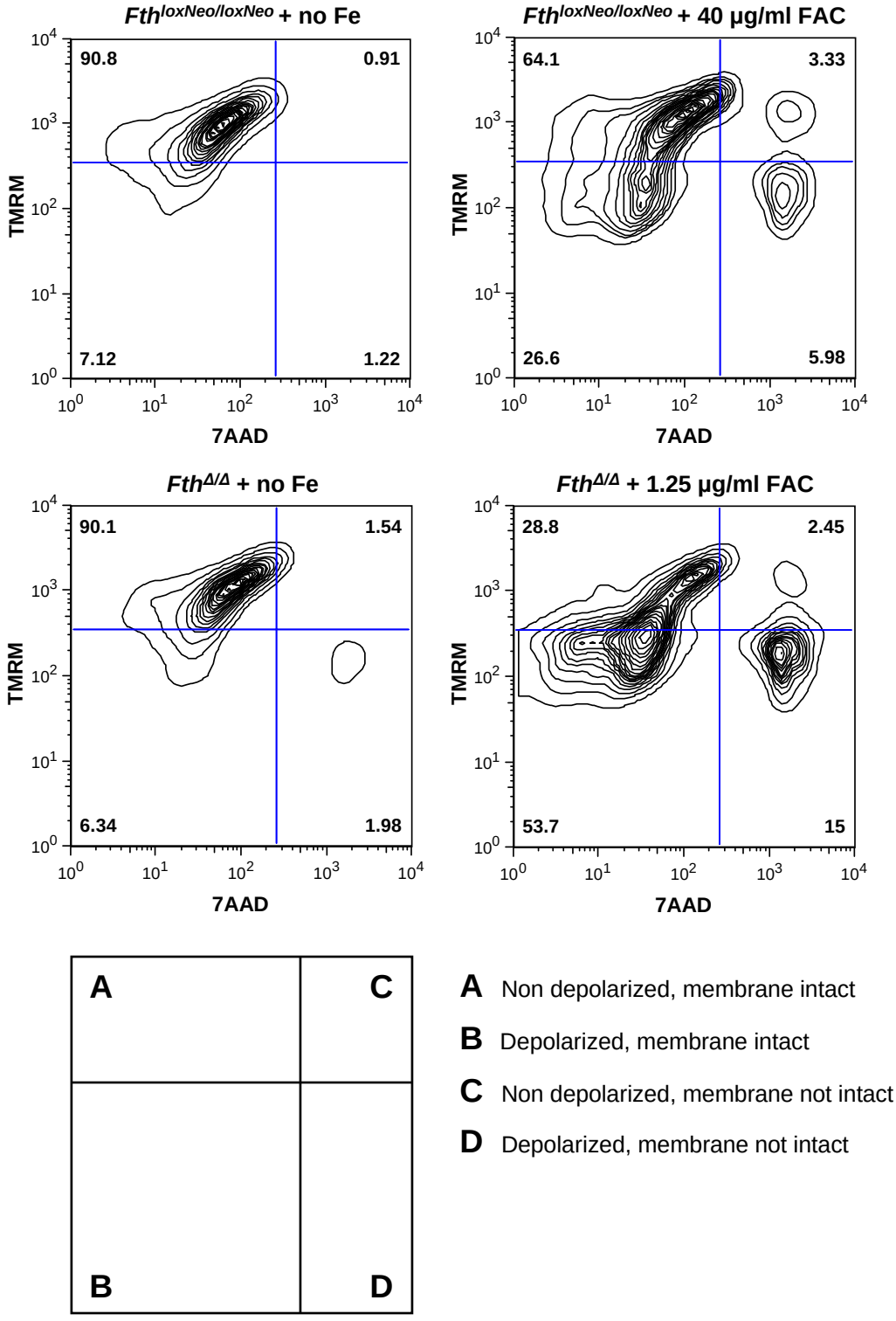

Supplementary figure 6. Assays of mitochondrial depolarization and cell membrane integrity. *Fth*$^{loxNeo/loxNeo}$ and *Fth*$^{Δ/Δ}$ cells were exposed to various concentrations of ferric ammonium citrate (FAC) for 3, 6 or 16 h. They were then stained with 250 nM tetramethyl rhodamine methyl ester (TMRM) and 2 µg/ml 7-amino-actinomycin D (7aaD) in order to measure the extent of mitochondrial depolarization and cell membrane integrity, respectively. Typical FACS profiles and the scoring is depicted. The results were expressed as % increase of cells in B (depolarized) and C plus D (membrane permeable). The summary of results are reported in Figure 5C.

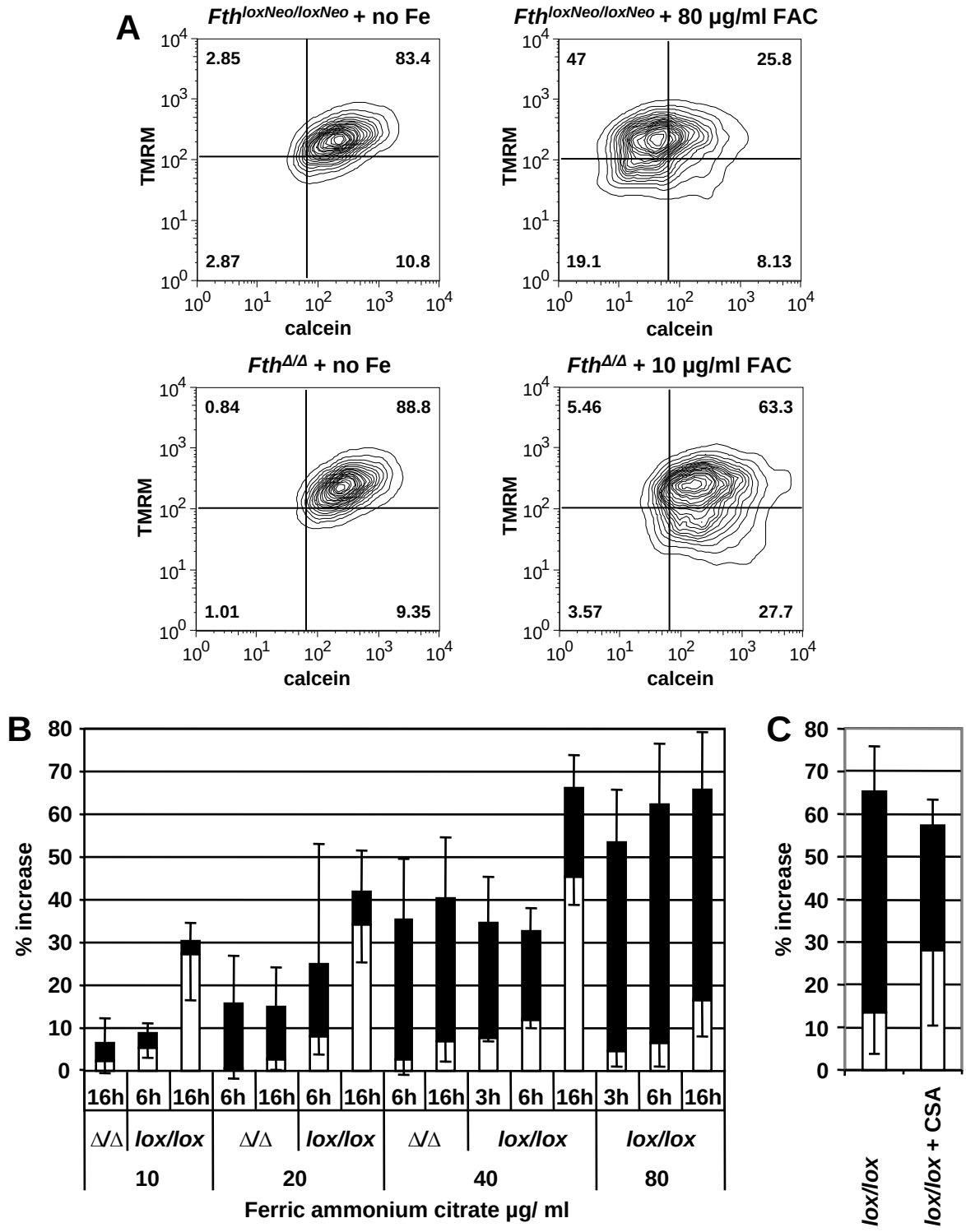

Supplementary figure 7. Measurements of mitochondrial permeability transition. *Fth*$^{loxNeo/loxNeo}$ and *Fth*$^{\Delta/\Delta}$ cells were exposed to various concentrations of ferric ammonium citrate for 3, 6 or 16 h. They were then stained with tetramethyl rhodamine methyl ester (TMRM), calcein AM/cobalt chloride, and 7-amino-actinomycin D (7aaD) to measure the extent of mitochondrial depolarization (white bars) and mitochondrial permeability transition (black bars) in 7aaD-negative cells, respectively. **A.** Typical FACS profiles. **B.** Graphical representation of all FACS data expressed as % increase in average fluorescence compared no addition of ferric ammonium citrate. **C.** Effect of cyclosporin A (CSA) on mitochondrial permeability transition *Fth*$^{loxNeo/loxNeo}$ cells treated with 80 µg/ml ferric ammonium citrate at 16 h. Note that cyclosporin A reduced the permeability transition, but increased the depolarization (n=3 at 3 h and 6 h; n=6 at 16 h).